Role of the antiparallel double-stranded filament form of FtsA in activating the *Escherichia coli* divisome

Abbigale Perkins[1], Mwidy Sava Mounange-Badimi[1], and William Margolin[1]

[1] Microbiology and Molecular Genetics, UTHealth McGovern Medical School, 6431 Fannin Street, Houston, TX 77030

*Corresponding author: william.margolin@uth.tmc.edu

ABSTRACT

The actin-like FtsA protein is essential for function of the cell division machinery, or divisome, in many bacteria including *Escherichia coli*. Previous *in vitro* studies demonstrated that purified wild-type FtsA assembles into closed mini-rings on lipid membranes, but oligomeric variants of FtsA such as FtsA^{R286W} and FtsA^{G50E} can bypass certain divisome defects and form arc and double-stranded (DS) oligomeric states, respectively, which may reflect conversion of an inactive to an active form of FtsA. Yet, it remains unproven which oligomeric forms of FtsA are responsible for assembling and activating the divisome. Here we used an *in vivo* crosslinking assay for FtsA DS filaments to show that they largely depend on proper divisome assembly and are prevalent at later stages of cell division. We also used a previously reported variant that fails to assemble DS filaments, FtsA$^{M96E\ R153D}$, to investigate the roles of FtsA oligomeric states in divisome assembly and activation. We show that FtsA$^{M96E\ R153D}$ cannot form DS filaments *in vivo*, fails to replace native FtsA, and confers a dominant negative phenotype, underscoring the importance of the DS filament stage for FtsA function. Surprisingly, however, activation of the divisome through the *ftsL** or *ftsW** superfission alleles suppressed the dominant negative phenotype and rescued the functionallity of FtsA$^{M96E\ R153D}$. Our results suggest that FtsA DS filaments are needed for divisome activation once it is assembled, but they are not essential for divisome assembly or guiding septum synthesis.

38 **IMPORTANCE**

39 Cell division is fundamental for cellular duplication. In simple cells like *Escherichia coli* bacteria,
40 the actin homolog FtsA is essential for cell division and assembles into a variety of protein
41 filaments at the cytoplasmic membrane. These filaments help to tether polymers of the tubulin-
42 like FtsZ to the membrane at early stages of cell division, but also play crucial roles in recruiting
43 other cell division proteins to a complex called the divisome. Once assembled, the *E. coli*
44 divisome subsequently activates synthesis of the division septum that splits the cell in two. One
45 recently discovered oligomeric conformation of FtsA is an antiparallel double stranded filament.
46 Using a combination of in vivo crosslinking and genetics, we provide evidence suggesting that
47 these FtsA double filaments have a crucial role in activating the septum synthesis enzymes.
48

INTRODUCTION

Bacterial cytokinesis relies on a dynamic protein nanomachine called the divisome, which is organized in a ring-like complex at mid-cell by the tubulin-like FtsZ protein (1–3). Actin-like FtsA protein plays a crucial role during early FtsZ-ring formation by anchoring FtsZ to the cytoplasmic membrane at the proto-ring stage (Fig. 1) and facilitating the recruitment of other essential divisome proteins (4, 5). Later in cytokinesis, synthesis of the division septum in most bacteria requires the action of the transmembrane proteins FtsW and FtsI, which harbor essential septal glycosyltransferase and transpeptidase activities, respectively, in their periplasmic domains (6–8). FtsWI in turn are recruited to the divisome by the FtsQLB transmembrane protein complex (9–11) and are kept in an inactive state by the periplasmic domains of FtsL and FtsB, collectively called constriction control domains (12). Thus, *E. coli* cell division features two temporally distinct stages (13): first assembly of the divisome machinery, then activation of FtsWI to synthesize the division septum.

Significant progress has been made recently in understanding how the *E. coli* divisome is assembled and FtsWI becomes activated. Hypermorphic alleles of FtsA, designated FtsA*, were initially found capable of bypassing the essential ZipA protein as well as other divisome defects (14–16). These FtsA* alleles were found to be deficient in oligomer formation compared with WT FtsA, according to two-hybrid studies (17). Subsequent *in vitro* studies demonstrated that purified FtsA forms closed 12-mer rings on lipid membranes, whereas FtsA* variants instead tended to assemble into arcs and other non-miniring structures, including double stranded (DS) filaments under certain conditions (18, 19). FtsA* also was shown in reconstitution experiments with FtsZ to form more dynamic structures on lipid membranes compared with WT FtsA (20). These biochemical and genetic studies suggested that FtsA oligomeric state regulates a divisome checkpoint, and disruption of FtsA minirings inactivates the checkpoint and allows FtsQLB and FtsWI to be recruited to the divisome (1, 17).

75 As mentioned above, FtsQLB themselves are key regulators of FtsWI activity. This was
76 initially revealed by hypermorphic alleles of FtsB and FtsL, designated FtsB* and FtsL*, which
77 harbor residue changes in their periplasmic domains that prematurely and constitutively activate
78 FtsWI (12, 21). The FtsQLB complex was later shown to be sufficient to promote FtsWI
79 enzymatic activity *in vitro* (6). In the periplasm, this activation is mainly mediated through a
80 domain in FtsL (AWI) that interacts with FtsI (22). Moreover, hypermorphic variants of FtsW and
81 FtsI, FtsW* and FtsI* have been isolated that mimic the activated state induced by FtsL* and
82 FtsB* (22–24), suggesting that FtsWI activation is the endpoint of these regulatory pathways.
83 Like the original FtsA* allele, these hypermorphic alleles of FtsL, FtsB, FtsW and FtsI promote
84 septum formation prematurely and at shorter cell lengths, resulting in significantly shorter cells
85 (12, 21, 25). Combinations of some of these hypermorphic alleles synergize to form nearly
86 spherical cells (12), presumably because the septum synthesis activity exceeds activity of the
87 elongasome, which is normally dominant and results in the rod shape of *E. coli* and other bacilli
88 (26, 27).
89 The prevailing model for how FtsA functions in *E. coli* cell division involves several
90 oligomeric state changes, which have been observed *in vitro* but largely only inferred *in vivo* (1,
91 28). In this model, FtsA initially self-interacts strongly to form minirings on the membrane (19,
92 29, 30). Upon a signal yet to be elucidated, it is postulated that these FtsA minirings are then
93 disrupted by interactions with the other essential FtsZ membrane anchor protein ZipA (31–33)
94 and perhaps other partners such as the divisome protein FtsX (34) or FtsQ (35) to form curved
95 oligomers (arcs) that, unlike minirings, seem to allow recruitment of downstream divisome
96 proteins, including FtsN.
97 The cytoplasmic domain of FtsN ($FtsN_{cyto}$), potentially in partnership with other divisome
98 proteins, interacts directly with FtsA (36, 37). Recently it was discovered that high
99 concentrations of purified $FtsN_{cyto}$ can convert FtsA minirings or arcs into DS filaments on lipid
100 membranes (30). These DS filaments are antiparallel, similar to DS filaments formed by another

101 bacterial actin homolog, MreB (30, 38) that guide the peptidoglycan synthesis machinery of the
102 elongasome to maintain the cylindrical shape of the bacterial cell wall (39). Notably, the FtsA^{G50E}
103 variant can form DS filaments on membranes constitutively, independently of FtsN$_{cyto}$ (19, 30).
104 This behavior suggested that FtsA^{G50E}, originally isolated as an FtsA*-like allele that suppressed
105 a thermosensitive allele of FtsA (FtsA^{S195P}) in *cis* (40), represents another activated oligomeric
106 form of FtsA. As the majority of FtsN is recruited at a late stage of divisome assembly and is
107 important for divisome activation (41, 42), it is attractive to propose that DS filaments reflect an
108 endpoint oligomeric state of FtsA that acts late in septum formation. Because they are curved
109 and oligomerize along the inner membrane surface, these DS filaments were postulated to be
110 crucial for guiding septum synthesis (30). Their antiparallel structure abrogates their ability to
111 treadmill, so Nierhaus et al. hypothesized that DS filaments guide septum synthesis by acting as
112 rudders to steer septal wall synthesis driven by FtsWI, analogous to the rudder mechanism
113 proposed to confer the spatial regulation of the elongasome by MreB DS filaments (30, 39).
114 In the present study, we ask whether these DS filaments of FtsA are required for physically
115 guiding septum synthesis, as proposed. We use site-specific cysteine crosslinking to show that
116 FtsA DS filaments form later in cell division and largely depend on divisome assembly,
117 consistent with the idea that DS filaments are mainly assembled close to the divisome activation
118 stage. We show that the DS filament-forming FtsA^{G50E} variant does not bypass ZipA very
119 efficiently compared with FtsA^{R286W}, consistent with the idea that DS filaments act at the later
120 activation stage. Moreover, we show that a variant of FtsA unable to form DS filaments is not
121 only non-functional in cell division but also exhibits a dominant negative phenotype, which
122 cannot be alleviated by incorporating FtsA*-like mutations. Surprisingly, however, this variant
123 can support normal divisome assembly and cell division if the divisome is activated by *ftsL** or
124 *ftsW** hypermorphic alleles. This leads us to conclude that although DS filaments of FtsA are not
125 essential for guiding septum synthesis, they play a key role in the activation of the divisome.
126

127 **RESULTS**

128

129 **Q155C can be used to detect the double stranded filament form of FtsA by *in vivo***
130 **crosslinking and does not affect normal FtsA functio**n. Previously, it was shown that
131 expression of the FtsA^{Q155C} variant could detect DS filaments of FtsA in *E. coli* cells by site-
132 specific cysteine crosslinking with another Q155C residue on the antiparallel FtsA filament (30).
133 As the distance between the Q155C residues in each FtsA filament is 12.6 Å in the atomic
134 structure (Fig. 2A), thiol crosslinkers with sufficiently long linker arms, such as BMH (13-16 Å) or
135 BMB (11 Å), could efficiently capture the interaction and resulted in a single prominent
136 crosslinked species on immunoblots from SDS-PAGE (30). Nierhaus et al. showed that this
137 *ftsA^{Q155C}* variant, fused to an internal 3X HA tag for immunodetection, was able to replace the
138 WT *ftsA* at the native locus of *E. coli*; these cells divided normally, indicating that the Q155C
139 residue change did not detectably affect FtsA function (30). We confirmed that when expressed
140 from a plasmid, FtsA^{Q155C} with an N-terminal FLAG tag (but lacking the 3X HA tag used
141 previously) can complement an *ftsA* null allele and confer normal cell division (data not shown
142 and see below). We then used this site-specific crosslinked band as a direct measure of the
143 prevalence of FtsA DS filaments in cells under various conditions.

144

145 **DS filaments of FtsA increase at later stages of division**. The prediction inferred from the
146 ability of FtsN$_{cyto}$ to convert FtsA minirings into DS filaments is that DS filaments appear later in
147 the septation process. To test this idea, we measured the prevalence of DS filaments during a
148 synchronized cell division time course. We achieved transient cell division synchrony by using
149 the well-known *ftsZ84*(ts) allele, which rapidly inactivates Z rings upon temperature shift to 42˚C
150 and rapidly restores them upon shift back to 30˚C (25). As a result of this restoration, divisomes
151 are rebuilt rapidly, and nondividing cells growing in rich medium such as LB generally begin
152 dividing again 20-30 minutes after the downshift (Fig. 2B and data not shown). We therefore

153 used these reactivation conditions to determine whether FtsA DS filaments assembled late
154 during the cell division cycle as hypothesized.

155 Cells with the *ftsZ84*(ts) allele and carrying pDSW210-FLAG-FtsA^{Q155C} were shifted to
156 42˚C to disassemble divisomes and then harvested for cysteine crosslinking 0, 10, and 20
157 minutes after returning to 30˚C. Protein samples from these time points were separated by
158 SDS-PAGE, followed by immunoblotting with anti-FtsA antibody to detect FtsA. We found that
159 the FtsA^{Q155C} crosslinked band, initially nearly undetectable, increased several-fold in intensity
160 over time at 30˚C, consistent with the assembly of most DS filaments at late stages of septation
161 (Fig. 2C,D). This band consistently migrated at ~125 kDa with SDS-PAGE, which is larger than
162 the predicted FtsA dimer size of ~90 kDa; however, unexpectedly slow migration of crosslinked
163 bands with SDS-PAGE is often observed with other *in vivo* crosslinking assays (43) and was
164 previously observed specifically with FtsA^{Q155C} (30).

165 To independently assess FtsA-FtsA interactions not directly involved in DS filaments, we
166 constructed FtsA^{S407C}, with a cysteine substitution in the amphipathic membrane targeting helix
167 (MTH) FtsA uses for binding to the membrane (4). Examination of high resolution tomograms of
168 negatively stained minirings on lipids suggests that these MTHs could potentially form an
169 internal ring inside the 20 nm-diameter miniring, potentially placing them in close contact with
170 each other (18). We also hypothesized that at least a subset of MTHs should similarly interact
171 with each other at the membrane surface when FtsA is assembled in other oligomeric
172 structures. Indeed, the immunoblots indicated that FtsA^{S407C} can efficiently crosslink with
173 FtsA^{407C} residues on other FtsA subunits when BMB or BMH crosslinkers are used, yielding
174 crosslinked bands at ~90 kDa, the expected size of an FtsA dimer (Fig. 2C). As with FtsA^{Q155C},
175 FtsA^{S407C} complemented an *ftsA* null mutant and allowed normal cell division (data not shown),
176 indicating that the serine to cysteine change did not appreciably disrupt the amphipathic nature
177 of the helix. Notably, whereas FtsA^{Q155C} crosslinking increased significantly upon resumption of
178 cell division, FtsA^{S407C} crosslinking remained relatively constant over time, indicating that the

179 observed increase in FtsA^{Q155C} crosslinking arises from specific FtsA-FtsA lateral interactions at
180 the DS filament interface and not from an overall increase in FtsA-FtsA interactions as cell
181 division progresses. We also tested another crosslinking residue, D123C, which like Q155C
182 detects DS filaments *in vivo* but with a much closer molecular interaction (~3.6 Å) (30). As a
183 result, this interaction cannot be detected by BMB or BMH but can be detected by the shorter
184 ~5 Å crosslinker dBBR (30). As with Q155C, we saw a 2-3-fold increase in crosslinking at
185 D123C after resumption of cell division in the *ftsZ84* strain, although the efficiency of
186 crosslinking was lower (Fig. S1).
187
188 **FtsA DS filaments depend on normal divisome assembly.** To provide more evidence that
189 DS filaments of FtsA form at a later stage of the cell division cycle, we asked whether DS
190 filament formation would be hindered by disrupting divisome assembly. To assess this, we
191 introduced pDSW210-FLAG-FtsA^{Q155C} into strains with *zipA1*(ts) or *ftsQ1*(ts) alleles, as both fail
192 to recruit downstream divisome proteins at the nonpermissive temperature of 42˚C (44–46). We
193 then compared the intensity of crosslinked bands on immunoblots at the permissive or
194 nonpermissive temperatures. Additionally, we included a strain carrying the pDSW210-FLAG-
195 FtsA^{Q155C} with an *ftsA* null allele in the chromosome as a control to account for the effects of
196 thermal induction.
197 When grown at 30˚C, all three strains displayed the expected prominent crosslinked
198 bands at ~125 kDa (Fig. 3). However, after shifting to 42˚C for 1 h, the intensities of the
199 crosslinked bands in the *zipA1* and *ftsQ1* mutants decreased 7.5-fold and 3-fold, whereas the
200 intensities of the bands in the complemented *ftsA* mutant remained nearly the same. As
201 essentially all *zipA1* and *ftsQ1* cells were highly filamentous at this time point at 42˚C (data not
202 shown), it is possible that the weak but detectable crosslinked protein bands represent DS
203 filaments that formed before the thermal shift, which failed to disassemble.

204 Overall, these data suggest that formation of FtsA DS filaments largely depends on
205 assembly of the divisome, at least up to the FtsQ-dependent step. As ZipA is important for
206 recruiting all divisome proteins downstream of FtsA and FtsZ and is postulated to be involved in
207 switching FtsA minirings to arcs and/or DS filaments, our results are consistent with this model.
208 They are also consistent with the increase in DS filaments at later stages of septation, as shown
209 above.
210
211 **Residue changes that promote or block FtsA DS filament formation *in vivo*.** We
212 hypothesized that the cysteine crosslinking assay should be able to detect higher levels of
213 crosslinking in cells expressing $FtsA^{G50E}$ compared to WT FtsA, assuming $FtsA^{G50E}$ forms DS
214 filaments constitutively *in vivo*. We therefore compared the crosslinked bands on immunoblots,
215 and indeed $FtsA^{G50E\ Q155C}$ reproducibly gave rise to more intense crosslinked protein bands at
216 ~125 kDa compared with $FtsA^{Q155C}$ alone (Fig. 4, Fig. S2). As a control, we tested whether the
217 presence of G50E affected the MTH-MTH interaction probed by crosslinking at S407C, but
218 there was no increase in band intensity at ~90 kDa (Fig. 4). This provides additional evidence,
219 already suggested by the time course of crosslinking depicted in Fig. 2, that the intensity of
220 crosslinked protein bands from $FtsA^{Q155C}$ can be used to assess the prevalence of DS filament
221 formation in the cell population.
222 We next wanted to test the effects of an FtsA variant reported to be defective in forming
223 DS filaments. This variant of FtsA, $FtsA^{M96E\ R153D}$, was previously designed based on the atomic
224 structure to inhibit interaction between two antiparallel FtsA filaments (Fig. 2A) (30). In that
225 study, a purified form of this variant formed robust minirings on lipid monolayers but, unlike WT
226 FtsA, was unable to form typical DS filaments *in vitro* upon addition of purified $FtsN_{cyto}$ (30).
227 To test the consequences of this defect on *E. coli* cell division, we first synthesized an
228 internal portion of the *ftsA* gene encoding these two residue changes and replaced the WT *ftsA*
229 in pSEB440, a medium copy plasmid with a *trc* promoter and relatively weak expression upon

230 IPTG induction (47, 48), with the double mutant insert. This plasmid was chosen because of
231 concerns that the double mutant might be dominant negative (see below). The double mutant
232 *ftsA*$^{M96E\ R153D}$ was also cloned into the higher-copy number plasmid pDSW210 so that it could be
233 expressed at higher levels from its P_{Trc} promoter for the cysteine crosslinking assays. Mutations
234 encoding the Q155C and S407C residue changes were incorporated into the pDSW210-
235 FtsA$^{M96E\ R153D}$ plasmid to create triple mutants for cysteine crosslinking *in vivo*. As we
236 suspected, cells carrying the pDSW210 derivatives of the double and triple mutants needed to
237 be grown on 0.2 % glucose to repress the P_{Trc} promoter, as the cells grew poorly otherwise,
238 likely due to a dominant negative effect of the double mutant (see below, and Fig. 5A).
239 Cysteine crosslinking experiments with FtsA$^{M96E\ R153D\ Q155C}$ and FtsA$^{M96E\ R153D\ S407C}$
240 derivatives showed that the ~125 kDa band that represents crosslinking between Q155C
241 residues in DS filaments was either undetectable or weak in repeat experiments (Fig. 4 and
242 data not shown), indicating that the M96E and R153D residue changes strongly block formation
243 of DS filaments *in vivo*. Crosslinking at S407C in the FtsA$^{M96E\ R153D}$ double variant was also
244 weaker compared to WT FtsA or FtsA^{G50E}, but still detectable (Fig. 4 and data not shown). We
245 conclude that the FtsA$^{M96E\ R153D}$ double variant largely fails to assemble DS filaments *in vivo*,
246 even when native FtsA is present.
247
248 **The dominant negative phenotype of FtsA$^{M96E\ R153D}$ is suppressed by superfission alleles.**
249 As mentioned above, FtsA$^{M96E\ R153D}$ derivatives were dominant negative, as certain strains could
250 not be transformed by pDSW210-FtsA$^{M96E\ R153D}$ in the absence of 0.2% glucose (Fig. 5A). This
251 dominant negative phenotype could be explained if some defective subunits interacting with WT
252 FtsA through longitudinal interactions prevented their co-assembly into DS filaments.
253 However, we hypothesized that perhaps a superfission allele such as *ftsL**, might
254 suppress the dominant negative phenotype by stimulating septum synthesis, as it can rescue
255 other cases of divisome inhibition (21, 22). Consistent with this idea, we found that pDSW210-

256 FtsA$^{M96E\ R153D}$ could efficiently be transformed into WM4953, which expresses *ftsL** from its
257 native chromosomal locus and is isogenic with the *ftsL*+ WM4952 strain (Fig. 5A).
258 We surmised that another potential way to suppress the dominant negative effect of the
259 double mutant was to incorporate G50E or R286W residue changes into the pDSW210-FtsA^{M96E}
260 ^{R153D} plasmid to make two new triple variants. However, despite the known capability of G50E
261 and R286W to suppress divisome defects, including suppression of other dominant negative
262 mutants (19, 48, 49), they were unable to suppress the M96E R153D alterations that block DS
263 filament formation. Instead, the triple variants remained dominant negative and failed to
264 transform WM4952 (Fig. 5A) when selected on LB agar without added glucose to repress
265 expression and under conditions where native FtsA was present (see below for additional
266 description of this strain).
267 The inability of the G50E alteration to suppress the FtsA$^{M96E\ R153D}$ dominant negative
268 effect is consistent with the idea that the G50E residue change, despite its ability to promote DS
269 filament formation in otherwise WT FtsA, does not have the capability to override the block to
270 DS filament formation caused by FtsA$^{M96E\ R153D}$. Moreover, the inability of R286W to suppress
271 the FtsA$^{M96E\ R153D}$ dominant negative phenotype suggests that FtsA needs to form DS filaments
272 in order to complete the stimulation conferred by the R286W allele. This contrasts with the
273 ability of the R286W residue change to suppress dominant negative alleles of FtsA such as
274 FtsA^{M71A} (49) probably because the latter may favor an oligomeric state that occurs earlier in the
275 process of cell division, such as divisome assembly, that is counteracted by R286W. In support
276 of this idea, FtsA^{M71A} forms DS filaments significantly less well than WT FtsA (~35% of WT
277 levels) as measured by *in vivo* crosslinking at Q155C, but introduction of the R286W residue
278 change to FtsA^{M71A} restores DS filament formation back to WT levels (Fig. S3).
279 As with the double variant, the triple variant constructs could be efficiently transformed
280 into the *ftsL** strain WM4953, allowing us to investigate their effects on cell division and viability
281 in more detail. We first asked whether FtsA$^{M96E\ R153D}$ retained any dominant negative effect in

282 the presence of *ftsL** compared with WT FtsA and the triple mutants. As seen in row 3 of the top
283 panels in Fig. 5B, the double mutant retained some dominant negative properties compared
284 with WT FtsA, which displayed no dominant negative effects at this induction level (row 2).
285 In contrast with the results from the *ftsL*+ WM4952 strain, the G50E or R286W residue
286 changes in the FtsA$^{M96E\ R153D}$ constructs in the *ftsL** WM4953 strain suppressed the dominant
287 negative effects when native FtsA was present (Fig. 5B top panels, rows 4-5). This suppression
288 by G50E or R286W was more pronounced than that achieved by *ftsL** alone, as shown by the
289 normal viability of both triple mutants at 100 μM IPTG. This suggests that *ftsL** synergizes with
290 G50E or R286W to compensate for the lack of FtsA DS filaments.
291
292 **The FtsA$^{M96E\ R153D}$ variant is unable to replace FtsA unless rescued by *ftsL****.We then asked
293 whether these FtsA variants were able to support cell division after native FtsA is depleted.
294 Strains WM4952 and WM4953 harbor an *ftsA* null (*ftsA*^{o}, frameshift) allele in the chromosome
295 and a low-copy plasmid that expresses WT *ftsA* from the bacteriophage lambda P_R promoter
296 along with its thermosensitive cI857 repressor. At temperatures >37˚C, the repressor is thermo-
297 inactivated, allowing WT FtsA to complement and cells to divide normally. However, shifting the
298 temperature to 30˚C or lower allows the repressor to inhibit P_R, which severely depletes FtsA
299 from cells (21), resulting in complete inhibition of cell division in the *ftsL*+ strain WM4952.
300 Previously it was shown that in WM4953 expressing the *ftsL** allele, when cellular FtsA
301 is significantly depleted by growth at 30˚C for several mass doublings, cell division is only mildly
302 impaired (21). This reduced requirement for FtsA may occur because divisome activation by
303 *ftsL** bypasses the requirement of most FtsA in the cell. Nonetheless, *ftsL** cannot bypass an
304 *ftsA*^{o} allele, indicating that some FtsA is still required for division in *ftsL** mutant cells (21),
305 probably because FtsA is needed at least for recruitment of FtsL to the divisome. Moreover, the
306 original *ftsL** allele (FtsL^{E88K}) cannot bypass the loss of ZipA either (data not shown),

307 presumably because ZipA is needed for recruitment of all downstream divisome proteins
308 including FtsL.
309 To assess the functionality of FtsA variants, we first expressed them from pDSW210
310 derivatives under conditions (growth at 30˚C) that depleted FtsA in either WM4952 or WM4953.
311 As expected, cells with the pDSW210 vector control lost viability but cells expressing WT FtsA
312 from pDSW210 retained normal viability (Fig. 5B, bottom panel, rows 1-2), even with no IPTG.
313 This was expected, as there is sufficient leaky expression from pDSW210 with no IPTG to
314 complement an *ftsA* null allele even in an *ftsL*+ strain (47). Notably, however, FtsA-depleted
315 *ftsL** cells expressing FtsA$^{M96E\ R153D}$ also exhibited normal viability with 0 or 25 μM IPTG, and
316 showed a slight dominant negative effect at 100 μM IPTG (Fig. 5B, bottom panels, row 3),
317 similar to the modest dominant negative effect in FtsA-replete cells mentioned above (Fig. 5B,
318 top panels, row 3). This suggests that the double mutant retains at least partial function,
319 provided that *ftsL** is present. Importantly, crosslinking experiments with the same FtsA$^{M96E\ R153D}$
320 variant expressed from pDSW210 showed that it remains deficient in forming DS filaments in
321 WM4953 (Fig. S2), ruling out the possibility that *ftsL** somehow allows restoration of DS filament
322 formation.
323 The FtsA$^{M96E\ R153D\ R286W}$ triple variant behaved similarly to the double variant, except
324 there was no dominant negative effect (Fig. 5B, bottom panels, row 5). This suggests that when
325 it is the main FtsA in the cell, the R286W variant synergizes with *ftsL** to bypass the block to DS
326 filament formation. We were surprised, however, to find that the FtsA$^{M96E\ R153D\ G50E}$ triple variant
327 grew poorly at several IPTG induction levels after FtsA depletion (Fig. 5B, bottom panels, row
328 4). This finding suggests that when it is in the predominant FtsA in cells harboring the *ftsL**
329 allele, the G50E residue change confers a dominant negative effect.
330 We then assessed the functionality of the FtsA variants when expressed from pSEB440,
331 which allowed for finer control of *ftsA* expression. We used IPTG to induce expression of the
332 different pSEB440-FtsA constructs under conditions (30˚C growth) that depleted FtsA. As

333 expected, depletion of native FtsA in *ftsL*+ WM4952 derivatives with the pSEB439 empty vector
334 resulted in no viability (Fig. 5C, row 1) and long filamentous cells (Fig. 5D, top panels). WT FtsA
335 restored full viability, but only after induction with IPTG (Fig. 5C row 2) and cell morphology was
336 normal upon IPTG induction (Fig. 5D, top panels). Notably, although FtsA$^{M96E\ R153D}$ and its triple
337 variant derivatives could be introduced into WM4952 because of lower expression levels, they
338 were unable to complement FtsA-depleted WM4952 even after IPTG induction (Fig. 5C, rows 3-
339 5), and formed long filamentous cells (Fig. 5C left panels, rows 3-5; Fig. 5D, top panels). These
340 results indicated that neither FtsA$^{M96E\ R153D}$ nor the addition of G50E or R286W changes can
341 replace native FtsA for function.
342 In contrast, in the *ftsL** WM4953 strain background, expression of FtsA$^{M96E\ R153D}$ or
343 FtsA$^{M96E\ R153D\ R286W}$ after depletion of native FtsA resulted in normal viability on spot dilution
344 plates (Fig. 5C right panels, rows 2,3,5), although this viability required IPTG induction (Fig. 5C,
345 right panels), unlike WT FtsA. FtsA$^{M96E\ R153D\ G50E}$ was slightly less viable (Fig. 5C right panels,
346 row 4), consistent with the negative synergy with *ftsL** observed in Fig. 5B.
347 To confirm that these detrimental effects on viability were due to cell division defects, we
348 compared the morphology of cells expressing FtsA$^{M96E\ R153D}$ or the triple variants to that of cells
349 expressing WT FtsA. Cells expressing FtsA$^{M96E\ R153D}$ or FtsA$^{M96E\ R153D\ R286W}$ divided, but less well
350 than those expressing WT FtsA, with about half of the cells showing some degree of elongation
351 (Fig. 5D, bottom panels 2, 3, 5). As predicted from the lower viability, cells expressing FtsA^{M96E}
352 $^{R153D\ G50E}$ (Fig. 5D, fourth bottom panel) formed longer filaments, consistent with the negative
353 synergy between G50E and *ftsL**.
354
355 **The FtsA$^{M96E\ R153D}$ variant can function as the sole FtsA in cells carrying the *ftsL** allele.** As
356 FtsA$^{M96E\ R153D}$ could allow cells with the *ftsL** allele to divide fairly well when WT FtsA was
357 depleted, we then asked if FtsA$^{M96E\ R153D}$ could function as the sole FtsA in the cell with no WT
358 FtsA present. Using a P1 phage lysate carrying a *leuA*::Tn*10* tetracycline resistance (tet^{R})

359 marker, which is ~50% linked to the *ftsA*^{o} allele by cotransduction (Fig. 6A), we transduced a
360 WT *ftsL*+ strain carrying pSEB440-FtsA$^{M96E\ R153D}$ to tet^R in the presence of 25-50 μM IPTG. We
361 found that 100% of tet^R transductants tested retained the WT *ftsA* allele, indicating that FtsA^{M96E}
362 ^{R153D} cannot function as the sole FtsA in an otherwise WT cell (data not shown) and consistent
363 with its inability to complement WM4952 under FtsA depletion conditions (Fig. 5C, D)
364 We then repeated the transductions, this time with a phage lysate carrying *leuA*::Tn*10*,
365 *ftsL** and *ftsA*^{o} in that gene order (from WM4953), such that 100% of tet^R recipients receiving
366 the *ftsA*^{o} allele would also acquire the *ftsL** allele (Fig. 6A). With a WT strain carrying pSEB440-
367 FtsA$^{M96E\ R153D}$ as recipient, we reproducibly isolated ~50% transductants that were dependent on
368 IPTG for full viability, indicating that the cells now required FtsA$^{M96E\ R153D}$ expressed from the
369 plasmid for survival. A representative sample of 4 transductants out of dozens tested is shown
370 in Fig. 6B. Microscopic examination of these cells revealed that 3 of the 4 were dependent on
371 IPTG for cell division, and we confirmed that these isolates (A, B, D in Fig. 6B) had the *ftsA*^{o}
372 allele and that the plasmid in these strains retained the FtsA$^{M96E\ R153D}$ residue changes (Fig. 6B
373 and data not shown). The ~50% cotransduction frequency of the *ftsA*^{o} allele with the *leuA::Tn10*
374 tet^R marker, as predicted from their 20 kb distance in the genome (Fig. 6A), also argues against
375 the acquisition of extragenic suppressors, as these would be expected to arise at frequencies
376 significantly lower than 50%.
377
378 **The FtsA$^{M96E\ R153D}$ variant is capable of recruiting FtsN to the divisome**. The ability of
379 FtsL* to allow the FtsA$^{M96E\ R153D}$ variant to function in cell division in the absence of WT FtsA
380 strongly suggests that FtsA$^{M96E\ R153D}$ can still successfully recruit downstream proteins, including
381 FtsL*, to the divisome. Nonetheless, it is possible that the FtsA$^{M96E\ R153D}$ variant, in the presence
382 of *ftsL**, might be able to bypass some of the normal divisome assembly pathway. We explored
383 this by testing if the late divisome protein FtsN could localize in *ftsA*^{o} *ftsL** cells that were
384 dependent on FtsA$^{M96E\ R153D}$ for division and viability. We introduced pSEB440-FtsA$^{M96E\ R153D}$ into

385 a strain expressing a GFP-FtsN fusion at its native chromosomal locus (XTL970), then
386 introduced the *ftsL** *ftsA*^{o} alleles into the chromosome by P1 transduction. The resulting strain
387 (WM7518) was confirmed by whole genome sequencing to carry *ftsL** and *ftsA*^{o} in the
388 chromosome and to carry pSEB440- expressing FtsA$^{M96E\ R153D}$ (data not shown). Complete
389 viability of this strain was dependent on IPTG (Fig. 7A), as expected, although partial viability
390 with no IPTG was also expected given the suppressing effects of *ftsL** on the amount of FtsA
391 required for cell division as described above.
392 Upon microscopic examination, we found robust GFP-FtsN fluorescent signals localized
393 at divisomes in essentially all the cells (Fig. 7B), both early during the division process as well
394 as in deeply constricting cells. This indicates that recruitment of later proteins by FtsA$^{M96E\ R153D}$ is
395 complete and suggests that FtsA-dependent recruitment of divisome proteins such as FtsN
396 does not depend on the DS filament form of FtsA. The clear localization of GFP-FtsN to sharply
397 constricting division septa also indicates that FtsN persists throughout cytokinesis, as is the
398 case in WT cells (Soderstrom et al. 2016).
399
400 **The defect in forming DS filaments can be rescued by either *ftsL*** or *ftsW** superfission**
401 **alleles expressed from plasmids.** To show independently that the *ftsL** superfission allele
402 could rescue the FtsA$^{M96E\ R153D}$ defect and be able to switch *ftsL** on when needed, we cloned a
403 strong *ftsL* superfission allele, *ftsL*$^{E88K\ G92D}$ (22), which we call *ftsL***, into the arabinose-inducible
404 plasmid pBAD18. We then evaluated its capacity to restore cell division in the *ftsL*+ WM4952
405 strain carrying pSEB440-FtsA$^{M96E\ R153D}$ after FtsA depletion at 30˚C and induction with
406 arabinose. A control strain expressing WT *ftsL* instead of *ftsL*** from pBAD18 was also included
407 for comparison.
408 We found that induction with IPTG and arabinose to express both FtsA$^{M96E\ R153D}$ and
409 FtsL** could fully rescue viability after FtsA depletion (Fig. 8A, bottom panels, row 2; Fig. 8B, left
410 panel, row 3) and resulted in normal division of most FtsA-depleted cells in the population (Fig.

411 8C, left panel). As expected, IPTG induction of FtsA$^{M96E\ R153D}$ alone did not help, and arabinose
412 induction of FtsL** alone only partially suppressed FtsA depletion, consistent with previous
413 observations that cells can divide with lower levels of FtsA when *ftsL** is present as mentioned
414 above (21). In contrast to FtsL**, expression of WT FtsL with arabinose did not rescue viability
415 of FtsA-depleted cells (Fig. 8A, bottom panels, row 2; Fig. 8C, left panel, row 2), and instead
416 conferred weaker growth of FtsA-replete cells (Fig. 8A, top panels, row 2), indicating that excess
417 WT FtsL is dominant negative. Overall, these data indicate that FtsA$^{M96E\ R153D}$ can support cell
418 division when FtsL** is co-produced.

419 The ability of *ftsL** or *ftsL*** to allow cell division independently of FtsA DS filaments
420 suggested that DS filaments normally function to activate FtsWI-mediated septum synthesis--a
421 role that can be bypassed if *ftsL** activates FtsWI instead. We therefore reasoned that a *ftsW** 422 superfission allele, which self-activates FtsWI, could also bypass the need for FtsA DS
423 filaments. We cloned the strong *ftsW** allele *ftsW^{E289G}* (Park et al. 2020) into the IPTG-inducible
424 pDSW210 plasmid and assayed its ability to rescue viability of cells expressing FtsA$^{M96E\ R153D}$
425 while depleted for native FtsA. Although low levels of IPTG (30 μM) were unable to rescue
426 viability of colonies on plates (Fig. 8A), high levels of IPTG (300 μM) could restore full viability
427 (Fig. 8B, C), suggesting that overexpression of *ftsW^{E289G}* could bypass the need for FtsA DS
428 filaments. These results indicate that both *ftsL** and *ftsW** superfission alleles can largely
429 bypass the need for FtsA DS filaments, consistent with the idea that DS filaments are needed
430 mainly for activation of FtsWI.

431 To confirm these results, we asked if FtsL** expressed from the pBAD18 plasmid could
432 support viability of cells expressing FtsA$^{M96E\ R153D}$ in the complete absence of WT FtsA. We
433 transformed WM7518, which harbors the *ftsL** and *ftsA^{o}* alleles in the chromosome and FtsA^{M96E}
434 ^{R153D} expressed from pSEB440, with pBAD18-FtsL**, and then introduced the Δ*ftsL::kan*
435 knockout allele by P1 transduction, selecting on IPTG and arabinose to express FtsA$^{M96E\ R153D}$
436 and FtsL**, respectively (Fig. 8D). All of the resulting transductants were arabinose-dependent

437 as expected, but importantly, half of them were dependent on IPTG for viability and half were
438 viable without IPTG (Fig. 8D), indicating that cell division depends on the expression of FtsA^{M96E}
439 ^{R153D}. (Half of the Δ*ftsL::kan* transductants are expected to become IPTG-independent because
440 the *ftsA*+ allele is ~50% cotransducible with Δ*ftsL::kan*). We obtained similar results when we
441 used WM7317 instead of WM7518 (data not shown). Interestingly, we were repeatedly unable
442 to introduce the *ftsA^o* allele by P1 transduction into strains harboring WT *ftsL* and expressing
443 both FtsL** and FtsA$^{M96E\ R153D}$ from plasmids under induction conditions (data not shown). In
444 summary, the viability of the Δ*ftsL::kan* strain complemented by pBAD18-FtsL** suggests that (i)
445 FtsL** produced from a plasmid can permit cell division in the absence of FtsA DS filaments and
446 (ii) WT FtsL somehow interferes with *ftsL** superfission alleles, at least in the case of correcting
447 FtsA DS filament defects.
448
449 **FtsA^{G50E} bypasses ZipA poorly compared with FtsA^{R286W}.** The FtsA^{G50E} allele, like other
450 FtsA*-like variants, can complement an *ftsA^o* allele and bypass ZipA (40). As ZipA is normally
451 essential for recruiting downstream divisome proteins, potentially through its role in the
452 disruption of FtsA minirings, this bypass of ZipA by FtsA^{G50E} is consistent with the latter being in
453 a non-miniring oligomeric state. However, FtsA^{G50E} differs from FtsA^{R286W} in that the former
454 seems to bypass the open arc form preferred by the latter variant. If the arc form is preferred for
455 recruitment of FtsK and other downstream divisome proteins, we wondered if the constitutive
456 DS filaments formed by FtsA^{G50E} might compromise its ability to bypass ZipA compared with
457 FtsA^{R286W}, particularly in a strain lacking any other source of FtsA.
458 To address this question, we used chromosomal *ftsA^o* strains carrying pDSW210
459 derivatives expressing FtsA^{R286W}, which should bypass ZipA efficiently; FtsA^{S195P}, a
460 thermosensitive variant which should fail to bypass ZipA even at the permissive temperature;
461 and FtsA^{G50E}, and transduced these with the Δ*zipA::kan* allele, selecting on plates containing
462 125 μM, 25 μM or 0 μM IPTG to assess the effects of different expression of the FtsA variants.

463 As expected, FtsA^{S195P} could not be transduced with Δ*zipA::kan* under any induction condition
464 (Fig. 9, bottom row), while FtsA^{R286W} transductants grew under all three conditions, but best with
465 some IPTG induction (Fig. 9, top row). Interestingly, FtsA^{G50E} did not yield transductants without
466 IPTG, and even with IPTG the transductants grew poorly compared to Δ*zipA::kan* mutants
467 expressing FtsA^{R286W}. Consistent with the observed colony phenotypes, cells of Δ*zipA::kan*
468 transductants expressing FtsA^{R286W} and grown in 50 μM IPTG were mostly normal in length,
469 whereas transductants expressing FtsA^{G50E} were uniformly filamentous (Fig. 9, right panels).
470 Higher induction levels of IPTG did not enhance the ability of FtsA^{G50E} to bypass ZipA and
471 instead inhibited growth (Fig. 9 and data not shown). These data suggest that when FtsA^{G50E} is
472 the sole FtsA in the cell, it has a weakened ability to recruit downstream proteins compared with
473 FtsA^{R286W}.
474
475 **DISCUSSION**
476
477 Here we have characterized the role of DS filaments of FtsA in *E. coli* cell division. We provide
478 evidence that DS filaments form late in the process of septation in *E. coli*, depend upon proper
479 divisome assembly, and are important for divisome activation. The FtsA$^{M96E\ R153D}$ variant,
480 previously reported to be deficient in forming DS filaments *in vitro* in response to FtsN$_{cyto}$, is
481 unable to complement an *ftsA* null allele *in vivo* and is strongly dominant negative. This is
482 consistent with the key role of DS filaments in FtsA's cell division functions, and the dominant
483 negative effect indicates that the loss of function of the FtsA$^{M96E\ R153D}$ variant is not due to
484 degradation, misfolding, or poor expression. Instead, we propose that the dominant negative
485 effect occurs because assembly and stability of DS filaments require most FtsA subunits to
486 interact at the lateral interface, and incorporation of even 1-2 subunits unable to form lateral
487 interactions can destabilize the entire DS filament.

488 The most compelling evidence for the role of FtsA DS filaments in divisome activation
489 comes from the ability of superfission alleles such as *ftsL** or *ftsW** to largely suppress the
490 dominant negative effects of FtsA$^{M96E\ R153D}$ and, even more strikingly, to allow it to function as
491 the main source of FtsA in the cell. Superfission alleles prematurely promote septum synthesis
492 by FtsWI, either by overriding normal signaling pathways from FtsQLB to FtsWI (*ftsL**) or by
493 self-activation (*ftsW**) (12, 21–23). Therefore, as superfission alleles can bypass the need for
494 FtsA DS filaments, it strongly suggests that DS filaments are normally involved in activating
495 FtsWI. Although the molecular mechanisms underlying this activation are unclear, the known
496 genetic interaction between FtsA and FtsW suggests that interaction between FtsA DS filaments
497 and the cytoplasmic loops of FtsW, most likely loop 2 (50), triggers conformational changes in
498 FtsW. It is attractive to postulate that these interactions in the cytoplasm, along with
499 conformational changes in the periplasmic domains of FtsW promoted by FtsQLB, FtsI and
500 FtsN, contribute synergistically to turn on FtsW's glycosyltransferase activity (51–53).
501 Our results are consistent with the following model. FtsA initially forms minirings on the
502 cytoplasmic membrane that represent a proto-ring checkpoint and are unable to recruit
503 downstream divisome proteins, possibly because they lack free termini (Fig. 10). Then,
504 responding to an unknown signal, ZipA and probably FtsX (33, 34) help to convert FtsA
505 minirings into an "early" arc oligomeric state of FtsA, represented by FtsA^{R286W}, which licenses
506 recruitment of downstream divisome proteins. This model then postulates that the distinct "late"
507 oligomeric state of FtsA is triggered by direct binding of FtsN$_{cyto}$ to the FtsA 1C subdomain (30,
508 36, 37, 48), which tips the equilibrium towards DS filament assembly (Fig. 10). This
509 conformational state is mimicked by FtsA variants such as FtsA^{G50E}. In this model, DS filaments
510 of FtsA are primed to activate FtsWI, likely by interacting more strongly with FtsW as described
511 above; importantly, these DS filaments may have lost their ability to recruit divisome proteins for
512 earlier stages of divisome assembly. The high levels of FtsN$_{cyto}$ required to convert FtsA into DS

513 filaments *in vitro* (30) suggests that other factors, including DS filaments themselves, may help
514 to promote this transition *in vivo*.
515 The ability of FtsA^{G50E} to bypass ZipA weakly, as opposed to not at all like WT FtsA,
516 suggests that the DS filaments are in equilibrium with arcs and that some arcs are present; this
517 is consistent with the small percentage of non-DS filaments on lipid monolayers previously
518 observed with purified FtsA^{G50E} (19, 30). Another possibility is that FtsA DS filaments can
519 facilitate back-recruitment of divisome proteins, perhaps through FtsN (48, 54), but that this
520 process is likely to be inefficient. The ability of FtsA^{G50E} to complement an *ftsA* null allele also
521 suggests that ZipA can convert DS filaments into a divisome-recruiting form, or, perhaps more
522 likely, that there are enough residual minirings (or other early structures) formed by FtsA^{G50E} that
523 can be converted into recruiting forms by ZipA or other proteins. Interestingly, two other
524 hypermorphic alleles of FtsA, FtsA^{I143L} and FtsA^{E124A}, can largely bypass FtsN under certain
525 conditions but are poor at bypassing ZipA (12, 16, 55). They share with FtsA^{G50E} a stronger
526 tendency to form DS filaments on lipid membranes *in vitro*, as lower concentrations of FtsN$_{cyto}$
527 are sufficient to convert minirings of FtsAI^{I143L} and FtsA^{E124A} to DS filaments compared with
528 FtsA^{R286W} (30). Moreover, FtsA^{Y139D}, which was previously isolated along with FtsA^{G50E} as a
529 suppressor of FtsA^{S195P}, forms a mixture of arcs and DS filaments, and like FtsA^{G50E} bypasses
530 ZipA less efficiently than FtsA^{R286W} (19, 40). This is consistent with the idea that FtsA arcs
531 bypass ZipA more readily than DS filaments. Despite their strong effects on FtsA
532 oligomerization, the inability of the G50E and R286W residue changes to rescue the block to DS
533 filaments caused by the M96E R153D lesions is consistent with the pathway shown in Fig. 10.
534 The negative synergy between G50E and *ftsL** is more difficult to explain, but may be related to
535 the mechanism by which G50E forms mostly DS filaments. G50 is located at the longitudinal
536 interface between FtsA subunits, and G50E therefore likely enhances lateral interactions
537 through an allosteric effect (19). It is possible that this mechanism allows only a small number of
538 FtsA arcs to be formed from minirings (see above) and thus perturbs recruitment of later

539 divisome proteins. As FtsAG50E can complement an *ftsA*^{o} allele, we speculate that a potential
540 imbalance of divisome proteins might still manage to synthesize the division septum but would
541 prone to failure if hyperstimulated by the *ftsL** allele. Clearly more studies of the costs of
542 bypassing divisome checkpoints are needed.

543 A previous model for FtsA DS filaments proposed that this oligomeric form might play a
544 role analogous to the DS filaments of MreB, which are postulated to act as rudders that sense
545 and respond to membrane curvature, thus shepherding cell wall synthases to work in spatially
546 restricted paths (28, 30, 39). In this analogy, DS filaments of FtsA would respond to the negative
547 curvature of the invaginating septal membrane, thus spatially restricting FtsWI and perhaps FtsZ
548 polymers to a narrow disc (30). This is an attractive model, particularly as it similar to the
549 proposed mechanism of SepF, another FtsZ membrane anchor conserved in Gram positive
550 bacteria and archaea, which can substitute for FtsA in *Bacillus subtilis* (5, 56, 57) and regulates
551 septal morphology (58). The prevalence of DS filaments of FtsA late in the cell division process,
552 observed in this study, is also consistent with the rudder model.

553 One of the corollaries of such a guiding mechanism for FtsA DS filaments is that they
554 should be essential for septum formation. Indeed, the failure of FtsA$^{M96E\ R153D}$ to complement an
555 *ftsA* null allele indicates that DS filaments are essential. However, the surprising ability of *ftsL**
556 or *ftsW** to bypass the requirement for DS filaments in cell division strongly suggests that their
557 essential function is to activate FtsWI, and not as a crucial membrane guide for septum
558 formation. It remains possible that other proteins have redundant roles with FtsA in guiding
559 septum formation in *E. coli*. Given that *E. coli* septum formation involves a fast-moving
560 treadmilling FtsZ track and a slower-moving septal synthase track comprising the FtsQLBWIN
561 proteins (52, 59), and that FtsA can interact with proteins in both tracks (20, 35, 59) it is
562 tempting to speculate that FtsA DS filaments may have a role in disengaging FtsQLBWIN from
563 the FtsZ track. This would help to trigger septal synthase activity and help to spatially regulate it
564 through an indirect mechanism.

565

566 **MATERIALS AND METHODS**

567

568 **Strains, plasmids, and growth conditions**. All strains and plasmids used for this study
569 are listed in Table S1 in the supplemental material. Bacterial cultures were grown with Lennox
570 lysogeny broth (LB) or agar plates unless otherwise indicated. Strains containing plasmids were
571 supplemented as needed with ampicillin (50 µg/ml), chloramphenicol (15 µg/ml), tetracycline (10
572 µg/ml), kanamycin (25 µg/ml), IPTG (various concentrations) or L-arabinose (0.2%). Optical
573 density of liquid cultures was assessed at 600 nm (OD_{600}). Strains for plasmid construction were
574 XL1-Blue, Top10, or WM7462 as detailed below.

575 **Construction of plasmids and strains.** All primers are listed in Table S2. Cysteine
576 substitutions at Q155C, S407C or D123C in *ftsA* were constructed by site-directed mutagenesis
577 using primers 2564 + 2565, 2634 + 2635, or 2931 and 2932, respectively, on plasmid pWM2785
578 (pDSW210-FLAG-FtsA). G50E or R286W changes were made by site-directed mutagenesis
579 using these derivatives as templates, with primers 2202 + 2203 for G50E and 2204 + 2205 for
580 R286W.

581 The mutant gene encoding $FtsA^{M96E\ R153D}$ was initially synthesized by Azenta Corp. as an
582 internal fragment of the *ftsA* open reading frame, spanning nucleotides 217-496, and cloned into
583 the pUC-GW-Kan plasmid vector. The internal *ftsA* gene fragment from this plasmid was the
584 source for replacing the WT *ftsA* sequences in pSEB440 by Gibson assembly using pSEB440
585 vector primers 2659 and 2660, and internal primers 2661 and 2662, resulting in pSEB440-
586 $FtsA^{M96E\ R153D}$ (pWM7215).

587 To achieve higher expression levels, the $ftsA^{M96E\ R153D}$ mutant gene from pWM7215 was
588 cloned into the high copy plasmid pDSW210 to make pWM7237. This was done by amplifying
589 the $ftsA^{M96E\ R153D}$ from pWM7215 with primers 2580 + 2581, cleaving with *Kpn* I + *Asc* I, and
590 cloning this fragment into plasmid pWM6246 (pDSW210-FtsA-$msfGFP^{sw}$) (47), which was

591 digested with *Kpn*I + *Asc*I (*Asc*I partial digestion, as there are two *Asc*I sites). The successfully
592 cloned insert was screened for the replacement of a large portion of the *ftsA* gene and its
593 msfGFP^{sw} insert with the smaller double mutant *ftsA* gene fragment lacking the msfGFP^{sw} insert
594 and verified by sequencing.

595 To construct a derivative of *ftsA*$^{M96E\ R153D}$ for *in vivo* cysteine crosslinking, we introduced
596 the Q155C change in the pDSW210-FLAG-FtsA derivative pWM7237 by site-directed
597 mutagenesis using primers 2735 and 2736, or the S407C change using primers 2739 and 2740.

598 Other mutant combinations were made by site-directed mutagenesis. To introduce
599 Q155C or S407C into FtsA^{G50E}, plasmid pWM5733 (pDSW210-FLAG-FtsA^{G50E}) was used as
600 template for site-directed mutagenesis with primers 2564 and 2634, respectively. Sequences of
601 pSEB440-FtsA derivatives were confirmed by sequencing the PCR product resulting from
602 pSEB440-specific primers 2814 and 2815. The M71A variant was introduced into pWM7049 or
603 pWM7239 by site-directed mutagenesis using primers 906 and 907.

604 To construct pBAD18-FtsL**, a DNA fragment containing the entire *E. coli ftsL* reading
605 frame encoding the E88K and G92D residue changes, along with flanking sequences from
606 upstream and downstream of the chromosomal *ftsL* gene including the *ftsL* translation initiation
607 site, was synthesized by Twist Bioscience, Inc. This fragment was then cloned downstream of
608 the P_{BAD} promoter on pBAD18-FtsL (pLD45) (60) by *in vivo* cloning in WM7462 (61), using
609 primers 2892 and 2893 to amplify the *ftsL*** gene and flanking sequences, and 2894 and 2895
610 to linearize the pBAD18 vector portion. To construct pDSW210-FtsW*, the entire *E. coli ftsW*
611 open reading frame encoding the E289G residue change was synthesized by Twist Bioscience,
612 Inc., and cloned into pDSW210 in frame with the ATG start codon in the vector by *in vivo*
613 cloning using primers 2877 and 2878 to linearize pDSW210, and 2879 and 2880 as internal
614 primers. The resulting plasmid expressed an N-terminally FLAG-tagged FtsW^{E289G} under P_{Trc}
615 control.

616 The replacement of chromosomal *ftsL* with the kan^R cassette was achieved by
617 recombineering, using the lambda Red-inducible strain DY329 (62) carrying pBAD18-FtsL
618 (pLD45). This strain (WM2406) was electroporated with a PCR product amplified from a kan^R
619 cassette and containing DNA flanking the *ftsL* gene using primers 712 + 713. Kan^R
620 transformants were selected in the presence of arabinose and verified by their dependence on
621 arabinose and by sequencing the junctions, and one strain was saved as WM2409. This strain
622 was used to make a P1 phage lysate carrying the Δ*ftsL::kan* allele that would be transduced into
623 WM7593 to make WM7594.
624 The absence of WT *ftsA* after transduction with WM4953 lysate was initially verified in
625 strains WM7317 and WM7518 by (i) the IPTG dependence of cell viability and (ii) amplification
626 of the chromosomal *ftsQ'-ftsA-ftsZ'* region from colony PCR confirming the lack of the unique
627 Bgl II site within the N-terminus of chromosomal *ftsA* due to the frameshift mutation that marks
628 the *ftsA^o* allele (Fig. 6A). These two strains were also subject to whole genome sequencing
629 (Plasmidsaurus, Inc.), which confirmed that they both harbor the *ftsL** and *ftsA^o* alleles in their
630 chromosomes and carried pSEB440 expressing FtsA$^{M96E\ R153D}$. This allowed us to conclude that
631 FtsA$^{M96E\ R153D}$ can replace WT FtsA provided that *ftsL** is present.
632 To construct the *ftsA^o ftsZ84*(ts) strain WM7412, WM1125 carrying pSEB440 was
633 transduced with P1 lysate from WM4952 (*leuA*::Tn*10 ftsA^o*), selecting for cm^R tet^R + IPTG.
634 Because >95% of transductants receiving the *ftsA^o* allele will also replace *ftsZ84*(ts) with *ftsZ*+,
635 100 transductants were screened for IPTG dependence and thermosensitivity. One transductant
636 was isolated that was both IPTG dependent and thermosensitive, and confirmed to be *ftsA^o*
637 *ftsZ84*(ts).
638 The failure of *ftsL** to bypass ZipA was tested by transducing WM2991 (*zipA1ts*) with P1
639 lysate from WM4953 carrying *ftsL** closely linked to the *leuA::Tn10* marker and selecting for tet^R
640 transductants at the permissive temperature of 30˚C. Six transductants were then inoculated
641 into LB broth + tetracycline and grown at 42˚C for several hours, then examined

642 microscopically. Cells in all six cultures were extremely filamentous. In addition, cells from the
643 transductant colonies were longer than normal, a feature of the *zipA1* allele and in contrast to
644 the very short cells typical of *ftsL** mutant strains.

645 Strains carrying pDSW210-FLAG-FtsA derivatives and a chromosomal *ftsA*^{o} allele
646 (WM4566, 4567, 4572) were grown at 30˚C and tested for their ability to bypass *zipA* by
647 transducing them with a Δ*zipA::kan* lysate derived from WM1657. Transductants were selected
648 on LB + ampicillin + kanamycin at 30˚C, supplemented with various concentrations of IPTG.
649 Transductants of the WM4566 and WM4572 strains were examined microscopically by
650 inoculating a single colony in corresponding liquid medium and growing until mid-logarithmic
651 phase.

652 **Serial dilution plating assays**. Overnight cultures were diluted 1:200 in fresh medium
653 and grown for 2-3 h under permissive conditions to an OD_{600} of 0.2 to 0.4. Cultures were
654 normalized by OD_{600} and then used to generate 10-fold serial dilutions in LB. Dilutions were
655 spotted (5 µl) onto LB agar plates containing the indicated concentrations of IPTG or L-
656 arabinose using a multichannel pipette. Plates were incubated overnight at temperatures
657 indicated and then imaged.

658 ***In vivo* cysteine crosslinking**. Overnight cultures were diluted 1:200 in fresh medium
659 containing 50-100 µM IPTG (for expressing various cysteine-substituted *ftsA* genes from
660 pDSW210) and grown to a final OD_{600} of 0.4 to 0.6 depending on the experiment. For the cell
661 division synchronization experiment using the *ftsZ84* mutant strains carrying pDSW210-FLAG-
662 FtsA, FtsA^{Q155C},FtsA^{S407C}, or FtsA^{D123C}, cultures were grown at 30˚C until an OD_{600} of 0.2, at
663 which point they were shifted to a 42˚C shaking water bath for 45 min, then shifted back to
664 30˚C. Aliquots from 0-, 10- and 20-min time points at 30˚C were placed on ice and processed
665 for crosslinking as described below. For the experiment with the *ftsA*^{o} allele and *ftsQ1* and *zipA1*
666 thermosensitive mutants, cultures were grown at 30˚C until an OD_{600} of 0.2, at which point they

667 were shifted to a 42˚C shaking water bath for 45 min prior to harvesting for crosslinking. For the
668 crosslinking experiment with WM4952 derivatives, cultures were all grown at 37˚C.
669 Cultures were placed on ice then the equivalent of 1.0 OD_{600} of each was pelleted,
670 washed with cold PBS, and resuspended in 50 µl cold PBS. BMB (1,4 bis-maleimidobutane)
671 and BMH (bis-maleimidohexane) crosslinkers (ThermoFisher Inc.) or dBBR (dibromobimane)
672 crosslinker (Sigma Aldrich) were prepared as 20 mM stock solutions in DMSO and added to
673 each resuspended cell pellet to a final concentration of 0.5 mM. After 10 min of incubation,
674 crosslinking was quenched by addition of 40 mM beta-mercaptoethanol (BME). Samples were
675 pelleted and resuspended in 36.4 µl of freshly prepared resuspension buffer (50 mM Bis-Tris pH
676 7.0, 750 mM aminocaproic acid, 2 mg/ml lysozyme, 1 mM EDTA, 1.43 mM BME, 1x EDTA-free
677 Pierce Protease Inhibitor [Thermo Scientific]) and incubated 20 min on ice. Dodecyl maltoside
678 and SDS were each added to a final concentration of 0.9%, followed by an additional 20 min
679 incubation on ice. Samples were then subjected to three cycles of 2-min incubation at 100˚C
680 followed by 2 min on dry ice, then pelleted in a microcentrifuge for 30 min. Supernatant fractions
681 (40 µl) were combined with 5X sample buffer (312 mM Tris pH 6.8, 10% SDS, 50% glycerol,
682 25% BME) and boiled for 3 min prior to SDS-PAGE. Wells were generally loaded with 5 µl, or
683 the equivalent of 0.1 OD_{600} of the original cell culture. Samples were stored at -20˚C.

684 **Immunoblot analysis.** Samples were boiled for 3 min prior to separation by SDS-
685 polyacrylamide gel electrophoresis (PAGE). Samples were transferred to nitrocellulose
686 membranes using a Mini Trans-Blot apparatus (Bio-Rad) at 200 mA for 55 min in Towbin
687 transfer buffer containing 0.1% SDS. Blots were stained by Ponceau staining to assess total
688 protein levels, then blocked using 3% bovine serum albumin (BSA) in Tris-buffered saline with
689 Tween 20 (TBST) and incubated with 1:5000 rabbit anti-FtsA or mouse anti-FLAG (F1804,
690 Sigma-Aldrich) antibodies. After washes, blots were incubated with 1:40,000 goat anti-rabbit-
691 HRP or anti-mouse-HRP, developed with Bio-Rad Clarity ECL substrate and imaged using a

692 Bio-Rad ChemiDoc MP system. The blots were also stained with Ponceau S (ThermoFisher) to
693 visualize the levels of loaded protein samples across lanes. Band intensities were quantitated
694 using ImageJ (63).

695 **Microscopy**. Overnight cultures were generally diluted 1:200 in liquid media and grown
696 to early or mid-logarithmic phase for imaging. Cells were either examined as wet mounts or
697 mounted on agarose pads and imaged on an Olympus BX63 microscope equipped with a
698 Hamamatsu C11440 ORCA-Spark digital complementary metal oxide semiconductor (CMOS)
699 camera using cellSens software (Olympus). Images were analyzed using Fiji/ImageJ (63).

700

701 ACKNOWLEDGMENTS

702 This work was supported by NIH grant GM131705 to W.M. and funding from the MD Anderson
703 UTHealth Graduate School of Biomedical Sciences to A.P. We thank Arindam Naha for initial
704 cloning of the synthesized FtsA double mutant fragment into pSEB439 by Gibson assembly,
705 Kara (Schoenemann) Hood and Brett Geissler for generating some of the strains and
706 preliminary data, Xin-tian Li for providing us with the XTL970 strain, Joe Lutkenhaus and
707 Sebastien Pichoff for providing us with the pSEB plasmids, Hironori Niki for providing the *in vivo*
708 cloning strain, and Todd Cameron, Daniel Haeusser and Lorenzo Suigo for helpful discussions
709 and advice.

710
711

712 **REFERENCES**
713

714 1. Cameron TA, Margolin W. 2024. Insights into the assembly and regulation of the bacterial
715 divisome. Nature Reviews Microbiology 22:33–45.

716 2. Levin PA, Janakiraman A. 2021. Localization, Assembly, and activation of the *Escherichia*
717 *coli* cell division machinery. 2. EcoSal Plus 9:eESP00222021.

718 3. Du S, Lutkenhaus J. 2019. At the heart of bacterial cytokinesis: The Z ring. Trends Microbiol
719 27:781–791.

720 4. Pichoff S, Lutkenhaus J. 2005. Tethering the Z ring to the membrane through a conserved
721 membrane targeting sequence in FtsA. Mol Microbiol 55:1722–1734.

722 5. Naha A, Haeusser DP, Margolin W. 2023. Anchors: a way for FtsZ filaments to stay
723 membrane bound. Mol Microbiol 120:525–538.

724 6. Marmont LS, Bernhardt TG. 2020. A conserved subcomplex within the bacterial cytokinetic
725 ring activates cell wall synthesis by the FtsW-FtsI synthase. Proc Natl Acad Sci U S A
726 117:23879–23885.

727 7. Wang L, Khattar MK, Donachie WD, Lutkenhaus J. 1998. FtsI and FtsW are localized to the
728 septum in *Escherichia coli*. J Bacteriol 180:2810–2816.

729 8. Taguchi A, Welsh MA, Marmont LS, Lee W, Sjodt M, Kruse AC, Kahne D, Bernhardt TG,
730 Walker S. 2019. FtsW is a peptidoglycan polymerase that is functional only in complex with
731 its cognate penicillin-binding protein. Nat Microbiol 4:587–594.

732 9. Buddelmeijer N, Beckwith J. 2004. A complex of the *Escherichia coli* cell division proteins
733 FtsL, FtsB and FtsQ forms independently of its localization to the septal region. Mol
734 Microbiol 52:1315–1327.

735 10. Craven SJ, Condon SGF, Díaz Vázquez G, Cui Q, Senes A. 2022. The coiled-coil domain of
736 *Escherichia coli* FtsLB is a structurally detuned element critical for modulating its activation
737 in bacterial cell division. J Biol Chem 298:101460.

738 11. Nguyen HTV, Chen X, Parada C, Luo A-C, Shih O, Jeng U-S, Huang C-Y, Shih Y-L, Ma C.
739 2023. Structure of the heterotrimeric membrane protein complex FtsB-FtsL-FtsQ of the
740 bacterial divisome. Nat Commun 14:1903.

741 12. Liu B, Persons L, Lee L, de Boer PA. 2015. Roles for both FtsA and the FtsBLQ
742 subcomplex in FtsN-stimulated cell constriction in *Escherichia coli*. Mol Microbiol 95:945–
743 970.

744 13. Aarsman ME, Piette A, Fraipont C, Vinkenvleugel TM, Nguyen-Disteche M, den Blaauwen
745 T. 2005. Maturation of the *Escherichia coli* divisome occurs in two steps. Mol Microbiol
746 55:1631–1645.

747 14. Geissler B, Margolin W. 2005. Evidence for functional overlap among multiple bacterial cell
748 division proteins: compensating for the loss of FtsK. Mol Microbiol 58:596–612.

749 15. Geissler B, Elraheb D, Margolin W. 2003. A gain of function mutation in *ftsA* bypasses the
750 requirement for the essential cell division gene *zipA* in *Escherichia coli*. Proc Natl Acad Sci
751 USA 100:4197–4202.

752 16. Bernard CS, Sadasivam M, Shiomi D, Margolin W. 2007. An altered FtsA can compensate
753 for the loss of essential cell division protein FtsN in *Escherichia coli*. Mol Microbiol 64:1289–
754 1305.

755 17. Pichoff S, Shen B, Sullivan B, Lutkenhaus J. 2012. FtsA mutants impaired for self-
756 interaction bypass ZipA suggesting a model in which FtsA's self-interaction competes with
757 its ability to recruit downstream division proteins. Mol Microbiol 83:151–67.

758 18. Krupka M, Rowlett VW, Morado DR, Vitrac H, Schoenemann KM, Liu J, Margolin W. 2017.
759 *Escherichia coli* FtsA forms lipid-bound minirings that antagonize lateral interactions
760 between FtsZ protofilaments. Nat Commun 8:15957.

761 19. Schoenemann KM, Krupka M, Rowlett VW, Distelhorst SL, Hu B, Margolin W. 2018. Gain-
762 of-function variants of FtsA form diverse oligomeric structures on lipids and enhance FtsZ
763 protofilament bundling. Mol Microbiol 109:676–693.

764 20. Radler P, Baranova N, Caldas P, Sommer C, López-Pelegrín M, Michalik D, Loose M. 2022.
765 In vitro reconstitution of *Escherichia coli* divisome activation. Nat Commun 13:2635.

766 21. Tsang MJ, Bernhardt TG. 2015. A role for the FtsQLB complex in cytokinetic ring activation
767 revealed by an ftsL allele that accelerates division. Mol Microbiol 95:925–944.

768 22. Park K-T, Du S, Lutkenhaus J. 2020. Essential Role for FtsL in activation of septal
769 peptidoglycan synthesis. mBio 11:e03012-20.

770 23. Li Y, Gong H, Zhan R, Ouyang S, Park K-T, Lutkenhaus J, Du S. 2021. Genetic analysis of
771 the septal peptidoglycan synthase FtsWI complex supports a conserved activation
772 mechanism for SEDS-bPBP complexes. PLoS Genet 17:e1009366.

773 24. Lariviere PJ, Mahone CR, Santiago-Collazo G, Howell M, Daitch AK, Zeinert R, Chien P,
774 Brown PJB, Goley ED. 2019. An essential regulator of bacterial division links FtsZ to cell
775 wall synthase activation. Curr Biol 29:1460-1470.e4.

776 25. Geissler B, Shiomi D, Margolin W. 2007. The *ftsA** gain-of-function allele of *Escherichia coli*
777 and its effects on the stability and dynamics of the Z ring. Microbiology 153:814–825.

778 26. Szwedziak P, Löwe J. 2013. Do the divisome and elongasome share a common
779 evolutionary past? Curr Opin Microbiol 16:745–751.

780 27. Egan AJ, Vollmer W. 2013. The physiology of bacterial cell division. Ann NY Acad Sci
781 1277:8–28.

782 28. Radler P, Loose M. 2024. A dynamic duo: Understanding the roles of FtsZ and FtsA for
783 *Escherichia coli* cell division through in vitro approaches. Eur J Cell Biol 103:151380.

784 29. Krupka M, Margolin W. 2018. Unite to divide: Oligomerization of tubulin and actin homologs
785 regulates initiation of bacterial cell division. F1000Res 7:235.

786 30. Nierhaus T, McLaughlin SH, Bürmann F, Kureisaite-Ciziene D, Maslen SL, Skehel JM, Yu
787 CWH, Freund SMV, Funke LFH, Chin JW, Löwe J. 2022. Bacterial divisome protein FtsA
788 forms curved antiparallel double filaments when binding to FtsN. Nat Microbiol 7:1686–
789 1701.

790 31. Hale CA, de Boer PA. 1997. Direct binding of FtsZ to ZipA, an essential component of the
791 septal ring structure that mediates cell division in *E. coli*. Cell 88:175–185.

792 32. Pichoff S, Lutkenhaus J. 2002. Unique and overlapping roles for ZipA and FtsA in septal
793 ring assembly in *Escherichia coli*. EMBO J 21:685-693.

794 33. Vega DE, Margolin W. 2019. Direct interaction between the two Z ring membrane anchors
795 FtsA and ZipA. J Bacteriol 201:e00579-18.

796 34. Du S, Pichoff S, Lutkenhaus J. 2016. FtsEX acts on FtsA to regulate divisome assembly
797 and activity. Proc Natl Acad Sci U S A 113:E5052-5061.

798 35. Baranova N, Radler P, Hernández-Rocamora VM, Alfonso C, López-Pelegrín M, Rivas G,
799 Vollmer W, Loose M. 2020. Diffusion and capture permits dynamic coupling between
800 treadmilling FtsZ filaments and cell division proteins. Nat Microbiol 5:407–417.

801 36. Busiek KK, Eraso JM, Wang Y, Margolin W. 2012. The early divisome protein FtsA interacts
802 directly through Its 1c subdomain with the cytoplasmic domain of the late divisome protein
803 FtsN. J Bacteriol 194:1989–2000.

804 37. Pichoff S, Du S, Lutkenhaus J. 2015. The bypass of ZipA by overexpression of FtsN
805 requires a previously unknown conserved FtsN motif essential for FtsA-FtsN interaction
806 supporting a model in which FtsA monomers recruit late cell division proteins to the Z ring.
807 Mol Microbiol 95:971–987.

808 38. van den Ent F, Izoré T, Bharat TA, Johnson CM, Löwe J. 2014. Bacterial actin MreB forms
809 antiparallel double filaments. eLife 3:e02634.

810 39. Hussain S, Wivagg CN, Szwedziak P, Wong F, Schaefer K, Izoré T, Renner LD, Holmes
811 MJ, Sun Y, Bisson-Filho AW, Walker S, Amir A, Löwe J, Garner EC. 2018. MreB filaments
812 align along greatest principal membrane curvature to orient cell wall synthesis. Elife
813 7:e32471.

814 40. Herricks JR, Nguyen D, Margolin W. 2014. A thermosensitive defect in the ATP binding
815 pocket of FtsA can be suppressed by allosteric changes in the dimer interface. Mol Microbiol
816 94:713–727.

817 41. Weiss DS. 2015. Last but not least: new insights into how FtsN triggers constriction during
818 *Escherichia coli* cell division. Mol Microbiol 95:903–909.

819 42. Gerding MA, Liu B, Bendezu FO, Hale CA, Bernhardt TG, de Boer PA. 2009. Self-enhanced
820 accumulation of FtsN at division sites and roles for other proteins with a SPOR domain
821 (DamX, DedD, and RlpA) in *Escherichia coli* cell constriction. J Bacteriol 191:7383–7401.

822 43. Cameron TA, Vega DE, Yu C, Xiao H, Margolin W. 2021. ZipA uses a two-pronged FtsZ-
823 binding mechanism necessary for cell division. mBio 12:e0252921.

824 44. Hale CA, de Boer PA. 2002. ZipA is required for recruitment of FtsK, FtsQ, FtsL, and FtsN
825 to the septal ring in *Escherichia coli*. J Bacteriol 184:2552-2556.

826 45. Weiss DS, Chen JC, Ghigo JM, Boyd D, Beckwith J. 1999. Localization of FtsI (PBP3) to the
827 septal ring requires its membrane anchor, the Z ring, FtsA, FtsQ, and FtsL. J Bacteriol
828 181:508–520.

829 46. Ghigo JM, Weiss DS, Chen JC, Yarrow JC, Beckwith J. 1999. Localization of FtsL to the
830 *Escherichia coli* septal ring. 2. Mol Microbiol 31:725–737.

831 47. Cameron TA, Margolin W. 2023. Construction and characterization of functional FtsA
832 sandwich fusions for studies of FtsA localization and dynamics during *Escherichia coli* cell
833 division. J Bacteriol 205:e0037322.

834 48. Pichoff S, Du S, Lutkenhaus J. 2018. Disruption of divisome assembly rescued by FtsN-
835 FtsA interaction in *Escherichia coli*. Proc Natl Acad Sci U S A 115:E6855–E6862.

836 49. Shiomi D, Margolin W. 2007. Dimerization or oligomerization of the actin-like FtsA protein
837 enhances the integrity of the cytokinetic Z ring. Mol Microbiol 66:1396–1415.

838 50. Park K-T, Pichoff S, Du S, Lutkenhaus J. 2021. FtsA acts through FtsW to promote cell wall
839 synthesis during cell division in *Escherichia coli*. Proc Natl Acad Sci U S A
840 118:e2107210118.

841 51. Britton BM, Yovanno RA, Costa SF, McCausland J, Lau AY, Xiao J, Hensel Z. 2023.
842 Conformational changes in the essential E. coli septal cell wall synthesis complex suggest
843 an activation mechanism. Nat Commun 14:4585.

844 52. Kashammer, L., Van Den Ent F, Jeffery M, Jean NL, Hale VL, Lowe J. 2022. Divisome core
845 complex in bacterial cell division revealed by cryo-EM. Nat Microbiol 8:1149-1159.

846 53. Attaibi M, den Blaauwen T. 2022. An updated model of the divisome: regulation of the septal
847 peptidoglycan synthesis machinery by the divisome. Int J Mol Sci 23:3537.

848 54. Goehring NW, Gueiros-Filho F, Beckwith J. 2005. Premature targeting of a cell division
849 protein to midcell allows dissection of divisome assembly in *Escherichia coli*. Genes Dev
850 19:127–137.

851 55. Goehring NW, Robichon C, Beckwith J. 2007. A role for the non-essential N-terminus of
852 FtsN in divisome assembly. J Bacteriol 189:646–649.

853 56. Ishikawa S, Kawai Y, Hiramatsu K, Kuwano M, Ogasawara N. 2006. A new FtsZ-interacting
854 protein, YlmF, complements the activity of FtsA during progression of cell division in Bacillus
855 subtilis. 6. Mol Microbiol 60:1364–1380.

856 57. Duman R, Ishikawa S, Celik I, Strahl H, Ogasawara N, Troc P, Lowe J, Hamoen LW. 2013.
857 Structural and genetic analyses reveal the protein SepF as a new membrane anchor for the
858 Z ring. 48. Proc Natl Acad Sci U S A 110:E4601–E4610.

859 58. Wenzel M, Celik Gulsoy IN, Gao Y, Teng Z, Willemse J, Middelkamp M, van Rosmalen
860 MGM, Larsen PWB, van der Wel NN, Wuite GJL, Roos WH, Hamoen LW. 2021. Control of

861 septum thickness by the curvature of SepF polymers. Proc Natl Acad Sci U S A
862 118:e2002635118.

863 59. Yang X, McQuillen R, Lyu Z, Phillips-Mason P, De La Cruz A, McCausland JW, Liang H,
864 DeMeester KE, Santiago CC, Grimes CL, de Boer P, Xiao J. 2021. A two-track model for
865 the spatiotemporal coordination of bacterial septal cell wall synthesis revealed by single-
866 molecule imaging of FtsW. Nat Microbiol 6:584–593.

867 60. Guzman LM, Weiss DS, Beckwith J. 1997. Domain-swapping analysis of FtsI, FtsL, and
868 FtsQ, bitopic membrane proteins essential for cell division in *Escherichia coli*. J Bacteriol
869 179:5094–5103.

870 61. Nozaki S, Niki H. 2019. Exonuclease III (XthA) enforces in vivo DNA cloning of *Escherichia*
871 *coli* to create cohesive ends. J Bacteriol 201:e00660-18.

872 62. Thomason LC, Costantino N, Li X, Court DL. 2023. Recombineering: Genetic engineering in
873 *Escherichia coli* using homologous recombination. Curr Protoc 3:e656.

874 63. Schneider CA, Rasband WS, Eliceiri KW. 2012. NIH Image to ImageJ: 25 years of image
875 analysis. Nat Methods 9:671–675.

876
877
878

879 **FIGURE LEGENDS**

880

881 **Fig. 1. Stages of cell division in *E. coli*.** A) Scheme of the cell division cycle, highlighting
882 stages relevant to this study. B) Essential divisome proteins, depicting the known FtsQLBWI
883 complex with FtsN, along with other divisome proteins at the membrane. The proto-ring
884 assembles first (i), followed by the remainder of the divisome (ii).

885

886 **Fig. 2*. In vivo* crosslinking detects an increase in FtsA DS filaments as cell division**
887 **progresses**. (A) Diagram of three FtsA subunits within an antiparallel DS filament (Nierhaus et
888 al. 2022) showing two green subunits in one filament and one orange subunit in the opposing
889 filament) and positions of residues described in this study, including the closely apposed Q155
890 residues that were replaced with cysteines and used for cysteine crosslinking by BMB or BMH
891 crosslinkers. The structure was derived from PDB 7Q6F. The BMB crosslinker structure is
892 depicted; BMH crosslinker is similar but spans 13 Å. S407 is part of the C-terminal membrane-
893 binding amphipathic helix and was not present in the crystal structure. (B) Scheme used to
894 synchronize *E. coli* cell division, using the *ftsZ84*(ts) allele. *E. coli ftsZ84*(ts) cells (WM1125)
895 were transformed with pDSW210FLAG-FtsA (negative crosslinking control), -FtsA^{Q155C} (detects
896 DS filaments by crosslinking between cysteines) or -FtsA^{S407C} (detects general FtsA-FtsA
897 intersubunit interactions through MTH-MTH interactions by cysteine crosslinking). After growth
898 at 30˚C to early logarithmic phase, cells were shifted to 42˚C to disrupt Z rings, then shifted
899 back to 30˚C to rapidly reassemble Z rings and restart the cell division cycle. C) Blot of samples
900 at various time points after shifting back to 30˚C, separated by SDS-PAGE and probed with anti-
901 FtsA antibody. DS filament crosslinks run at ~125 kDa, whereas MTH-MTH crosslinks run at the
902 FtsA dimer size of ~90 kDa. Note that the lower levels of FLAG-FtsA compared with FtsA is in
903 part a result of cleavage of the FLAG tag from the plasmid-expressed version. A portion of the
904 Ponceau S-stained blot is shown below the immunoblot, along with relative intensities of the

905 crosslinked band normalized to the zero minute time point. D) Blot from an independent
906 experiment using cells from strain WM7547 carrying pDSW210FLAG-FtsA^{Q155C} introduced into
907 the *ftsA^o ftsZ84*(ts) strain WM7412, with the same protocol as in (B), showing a similar increase
908 in crosslinking over time. A portion of the Ponceau S-stained blot is shown below the
909 immunoblot, along with relative intensities of the crosslinked band normalized to the zero minute
910 time point for each Q155C or S407C time point experiment shown.
911
912 **Fig. 3. DS filament formation depends on divisome assembly.** Derivatives of plasmid
913 pDSW210-Flag-FtsA^{Q155C} were introduced into *ftsQ1ts* (WM7148), *zipA1ts* (WM7149) or
914 combined with an *ftsA^o* allele (WM7150), grown at 30˚C until early logarithmic phase, then split
915 into 30˚C or 42˚C cultures for an additional hour prior to cysteine crosslinking before SDS-PAGE
916 and immunoblotting with anti-FtsA. A portion of the Ponceau S-stained blot is shown below the
917 immunoblot.
918
919 **Fig. 4. FtsA$^{M96E\ R153D}$ is defective in forming DS filaments *in vivo*.** Derivatives of plasmid
920 pDSW210-FtsA^{Q155C} and/or FtsA^{S407C} in WM4952 carrying no additional residue changes (WT)
921 or additional residue changes as shown, were assayed by *in vivo* cysteine crosslinking to
922 identify DS filaments or MTH-MTH interactions, respectively. BMH was used as crosslinker.
923 Crosslinked samples were separated by SDS-PAGE followed by immunoblotting with anti-FtsA.
924 A portion of the Ponceau S-stained blot is shown below the immunoblot. All plasmid-expressed
925 FtsA derivatives possess an N-terminal FLAG tag except for FtsA$^{M96E\ R153D}$. The several larger
926 crosslinked bands in the final lane suggest that FtsA protein carrying both Q155C S407C
927 alterations can form both longitudinal and lateral crosslinks that result in higher-molecular
928 weight structures.
929

930 **Fig. 5. FtsA$^{M96E\ R153D}$ is dominant negative and is unable to complement native FtsA except**
931 **in the presence of the *ftsL** allele.** *A*) Strains WM4952 (*ftsL*+, top row) or WM4953 (*ftsL**,
932 bottom row) were transformed with pDSW210 vector or pDSW210 expressing WT or mutant
933 FtsA derivatives (top), with no IPTG added, to maintain basal levels of expression. Images were
934 taken after overnight incubation at 37˚C. No transformants expressing FtsA$^{M96E\ R153D}$ were
935 obtained, even at uninduced levels of IPTG, unless the *ftsL** allele was present in the
936 chromosome (WM4953) instead of *ftsL*+ (WM4952). The presence of G50E or R286W
937 superfission alleles in *cis* did not permit viability without *ftsL**. B) Dominant negative effects of
938 strains with *ftsL** and expressing WT FtsA or the mutant combinations from pDSW210 were
939 tested at several different IPTG induction levels, with normal levels of native FtsA or depleted
940 for native FtsA. In *ftsL** cells with normal levels of native FtsA (upper images), the dominant
941 negative phenotype of FtsA$^{M96E\ R153D}$, already strongly suppressed by *ftsL** as shown in (B), was
942 further suppressed by R286W or G50E (detectable at 100 μM IPTG). When FtsA was depleted,
943 FtsA$^{M96E\ R153D}$ and FtsA$^{M96E\ R153D\ R286W}$ strains were viable. However, when forced to be the sole
944 functional FtsA, FtsA$^{M96E\ R153D\ G50E}$ did not support viability, suggesting that the G50E allele is
945 synthetically sick when combined with *ftsL*.* C) Controlled expression of FtsA and variants from
946 pSEB439/pSEB440 after depletion of native FtsA in WM4952. WM4952 (*ftsL*+) or WM4953
947 (*ftsL**) cells carrying pSEB439 vector or expressing FtsA (pSEB440) or FtsA variants
948 (pWM7215, pWM7496, pWM7522) were diluted and spotted onto agar plates and incubated at
949 30˚C to deplete native FtsA, with either no IPTG or 100 μM IPTG to induce expression of the
950 FtsA variants from the plasmid. D) Top row: Micrographs of overnight cultures of WM4952 at
951 30˚C carrying pSEB440 derivatives as noted (+ 55 μM IPTG added to induce plasmid-
952 expression of FtsA derivatives), indicating that FtsA$^{M96E\ R153D}$ cannot substitute for native FtsA.
953 Bottom row: same as top row except the strain background is the isogenic *ftsL** strain WM4953,
954 which allows FtsA$^{M96E\ R153D}$ and its derivatives to divide, although not completely normally. Scale
955 bar, 10 μm.

956

957 **Fig. 6. FtsA$^{M96E\ R153D}$ can completely replace native FtsA in the cell when *ftsL** is present.**
958 (A) Scheme for P1 phage co-transduction of *ftsL** and *ftsA^o* with the *tet^R leuO*::Tn*10* marker
959 from WM4953 P1 lysate into a WT strain carrying pSEB440-FtsA$^{M96E\ R153D}$. The *ftsA^o* and *ftsL**
960 alleles are ~90% and 50% linked to tetR, respectively. Double recombination necessary for
961 cotransduction of *ftsA^o* and *ftsL** alleles is denoted by X's. The resulting Cm^R Tet^R transductant
962 lacks WT *ftsA* and depends on FtsA$^{M96E\ R153D}$ for viability. (B) Presence or absence of the *ftsA^o*
963 allele in four transductants from the experiment outlined in (A) confirmed by IPTG-dependence
964 (patches of cells on LB agar ± IPTG, top) or Bgl II digested PCR products of chromosomal *ftsA*
965 from transductant colonies (gel image, bottom). Isolates A, B and D have acquired *ftsA^o*, and
966 thus also must have acquired *ftsL** by cotransduction according to the scheme in (A).
967

968 **Fig. 7. FtsA DS filaments are not required for divisome assembly or recruitment of FtsN.**
969 Strain WM7518 carries pSEB440-FtsA$^{M96E\ R153D}$, expresses a GFP-FtsN fusion at the native *ftsN*
970 chromosomal locus and harbors the *ftsL** and *ftsA^o* alleles introduced by P1 transduction. (A)
971 Confirmation that normal viability of WM7518 requires IPTG-dependent expression of FtsA^{M96E}
972 ^{R153D}, indicating that it is driving cell division in the absence of native FtsA. (B) The GFP-FtsN
973 fusion localizes to nearly all divisomes in cells relying on FtsA$^{M96E\ R153D}$ and *ftsL** for division.
974 Two representative fields of cells (DIC and fluorescence) are shown, highlighting GFP-FtsN
975 localization at early (arrows) or late (arrowheads) stages of septation. Scale bar, 5 μm.
976

977 **Fig. 8. Superfission *ftsL*** or *ftsW** alleles expressed from plasmids allow FtsA$^{M96E\ R153D}$ to**
978 **replace native FtsA.** A) Plasmid pSEB440-FtsA$^{M96E\ R153D}$ was introduced into the FtsA
979 depletion strain WM4952 in combination with pDSW210-FtsA* (R286W, strain WM7599),
980 pBAD18-FtsL (strain WM7600), pBAD18-FtsL** (E88K G92D, strain WM7539), or pDSW210-
981 FtsW* (E289G, strain WM7540). Mid-logarithmic phase cultures grown at 37˚C were serially

982 diluted and spotted onto agar plates containing the inducers shown and incubated overnight at
983 37˚C to maintain expression of the native FtsA, or 30˚C to deplete native FtsA. IPTG is needed
984 to express FtsA$^{M96E\ R153D}$ or FtsW* from pSEB440 or pDSW210 plasmid, respectively. L-
985 arabinose (Ara) is required to express FtsL or FtsL** from their plasmids. Full complementation
986 by FtsA$^{M96E\ R153D}$ after FtsA depletion was achieved with arabinose induction of FtsL** in
987 combination with IPTG. There was sufficient leaky expression of FtsA* from pDSW210 to
988 complement with no inducer. B) Induction of FtsL** with only arabinose partially rescued
989 viability, but high level IPTG induction (300 μM) of FtsW* fully rescued viability. C) WM4952
990 derivatives with the plasmids indicated were grown in 30 μM IPTG + 0.2% arabinose at 30˚C for
991 3.5 hours prior to imaging. Representative fields of cells are shown, after merging DIC and GFP
992 channels. WM4952 expresses ZapA-GFP, a proxy for the Z ring (arrows), from its native locus.
993 The short cell lengths for FtsL** and the mixture of short cells and moderate cell filamentation
994 for FtsW* with 30 μM IPTG are consistent with the spot dilution results. Scale bar, 10 μm. D)
995 FtsL** expressed from an arabinose-inducible promoter on a plasmid allows FtsA$^{M96E\ R153D}$ to be
996 the sole source of FtsA. A schematic for Δ*ftsL::kan* transduction of WM7593 (*ftsL* ftsA^{o}*
997 pSEB440- FtsA$^{M96E\ R153D}$ pBAD18-FtsL**) to replace the chromosomal *ftsL** allele with Δ*ftsL::kan*
998 is shown at the left; crossovers that would result in Δ*ftsL::kan ftsA^{o}* transductants (~50%
999 cotransduction frequency) are depicted. Eight transductants were picked at random and
1000 streaked on selective agar with or without IPTG (30 μM) or arabinose (0.2%) and incubated
1001 overnight at 30˚C (shown at the right). All eight transductants were arabinose dependent; half
1002 (highlighted with stars) were IPTG dependent and thus depended on both FtsL** from pBAD18-
1003 FtsL** and FtsA from pSEB440-FtsA$^{M96E\ R153D}$ for viability.
1004
1005 **Fig. 9. FtsA^{G50E} weakly bypasses ZipA compared with FtsA^{R286W}.** Strains WM4566, 4567
1006 and 4572 were transduced with Δ*zipA::kan* P1 lysate and plated on LB Amp Kan plus
1007 concentrations of IPTG shown to express the various FtsAs from plasmids and incubated at

1008 37˚C overnight prior to imaging the agar plates. To examine cell morphology, one Δ*zipA::kan*
1009 transductant from $FtsA^{G50E}$ or $FtsA^{R286W}$ was inoculated in broth and grown in LB Amp Kan broth
1010 supplemented with 50 μM IPTG until reaching an OD_{600} of ~0.5 ($FtsA^{R286W}$) or 0.1 ($FtsA^{G50E}$,
1011 which was concentrated ~5x prior to viewing). Scale bar, 10 μm.
1012
1013 **Fig. 10. Proposed model of the effects of FtsA oligomeric states on divisome assembly**
1014 **and activation**. FtsA minirings, arcs and DS filaments are shown above the proposed
1015 assembly/activation state of the divisome they affect, along with variants that favor the various
1016 FtsA oligomeric states. Note that there is no direct evidence yet for the existence of FtsA
1017 minirings and arcs *in vivo*. Mutants that block transitions between states are shown at the
1018 bottom.
1019

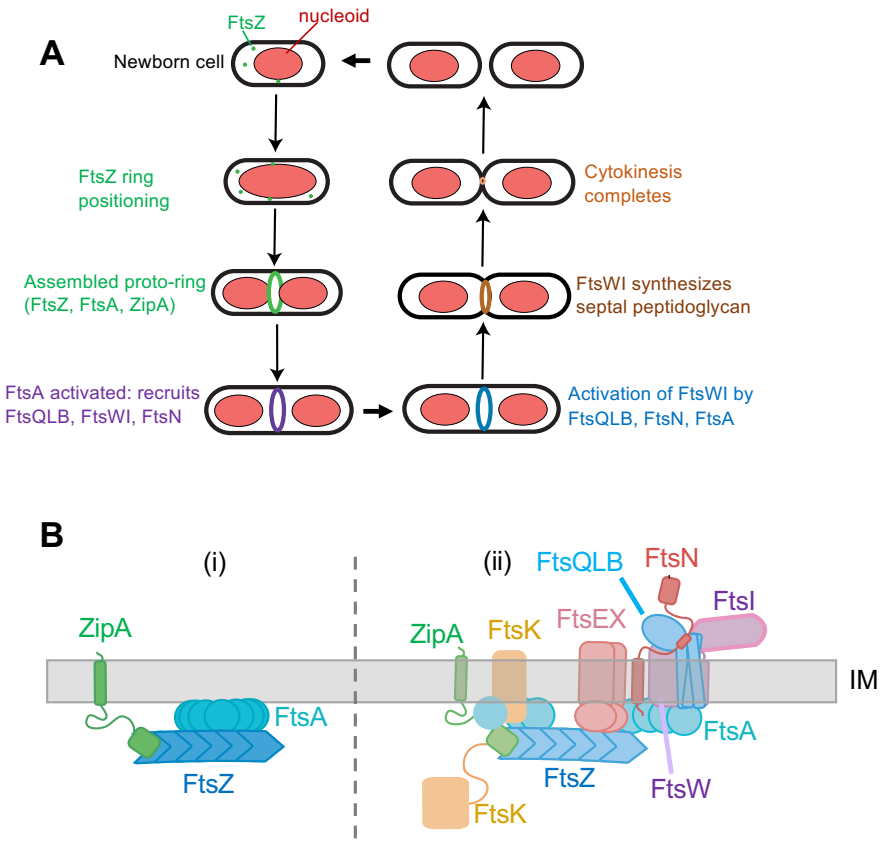
A
FtsZ
nucleoid
Newborn cell
FtsZ ring positioning
Assembled proto-ring (FtsZ, FtsA, ZipA)
FtsA activated: recruits FtsQLB, FtsWI, FtsN
Activation of FtsWI by FtsQLB, FtsN, FtsA
FtsWI synthesizes septal peptidoglycan
Cytokinesis completes
B
(i)
ZipA
FtsA
FtsZ
(ii)
FtsQLB
FtsN
FtsI
ZipA
FtsK
FtsEX
IM
FtsA
FtsZ
FtsW
FtsK

Fig. 1

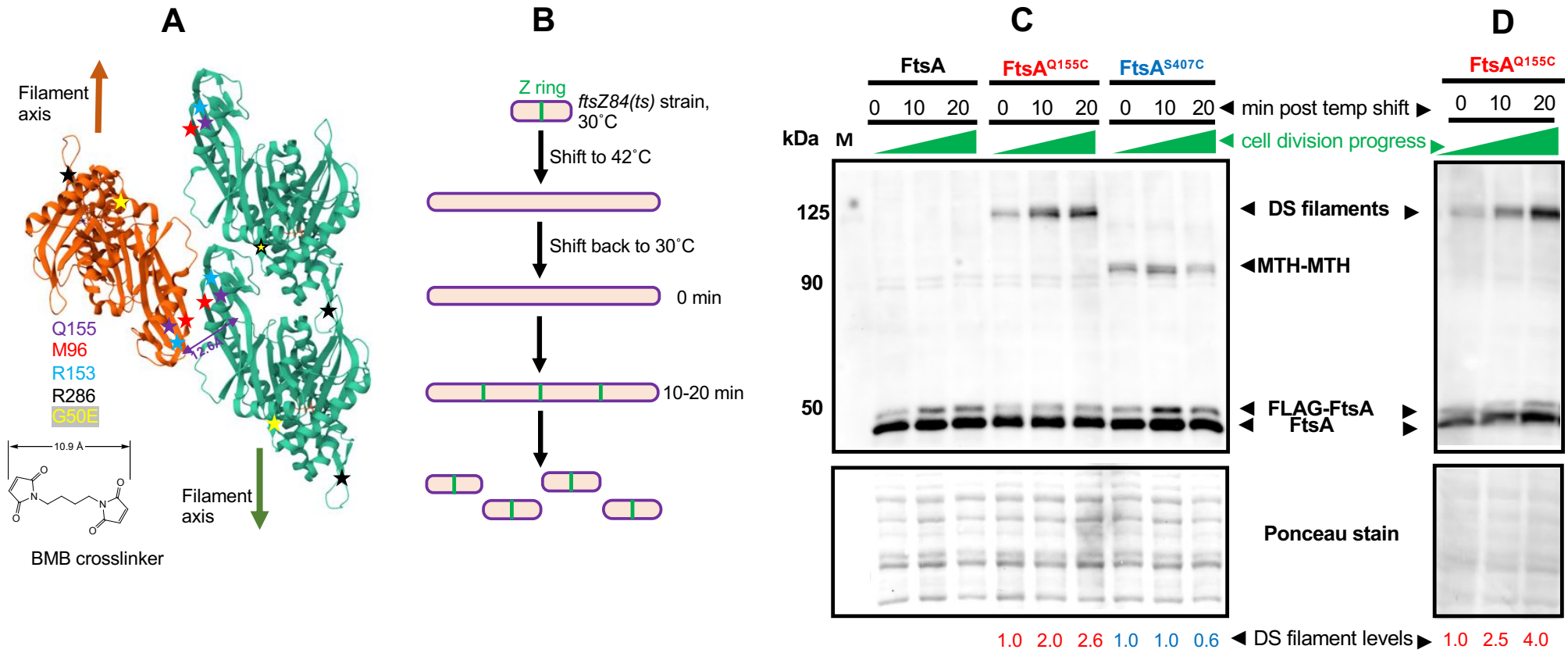
A
Filament axis
Q155
M96
R153
R286
G50E
10.9 Å
BMB crosslinker
Filament axis
B
Z ring
ftsZ84(ts) strain, 30˚C
Shift to 42˚C
Shift back to 30˚C
0 min
10-20 min
C
FtsA
FtsAQ155C
FtsAS407C
0 10 20 0 10 20 0 10 20
min post temp shift
cell division progress
kDa M
125
90
50
DS filaments
MTH-MTH
FLAG-FtsA
FtsA
Ponceau stain
1.0 2.0 2.6 1.0 1.0 0.6
DS filament levels
D
FtsAQ155C
0 10 20
1.0 2.5 4.0

Fig. 2

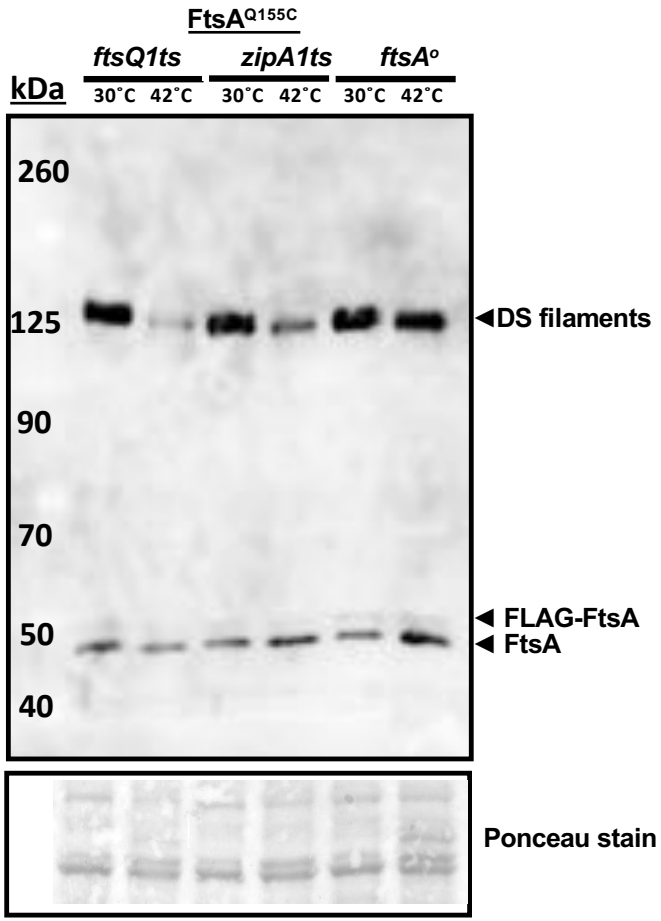
FtsA^Q155C
ftsQ1ts
zipA1ts
ftsA°
kDa
30°C 42°C 30°C 42°C 30°C 42°C
260
125
90
70
50
40
DS filaments
FLAG-FtsA
FtsA
Ponceau stain

Fig. 3

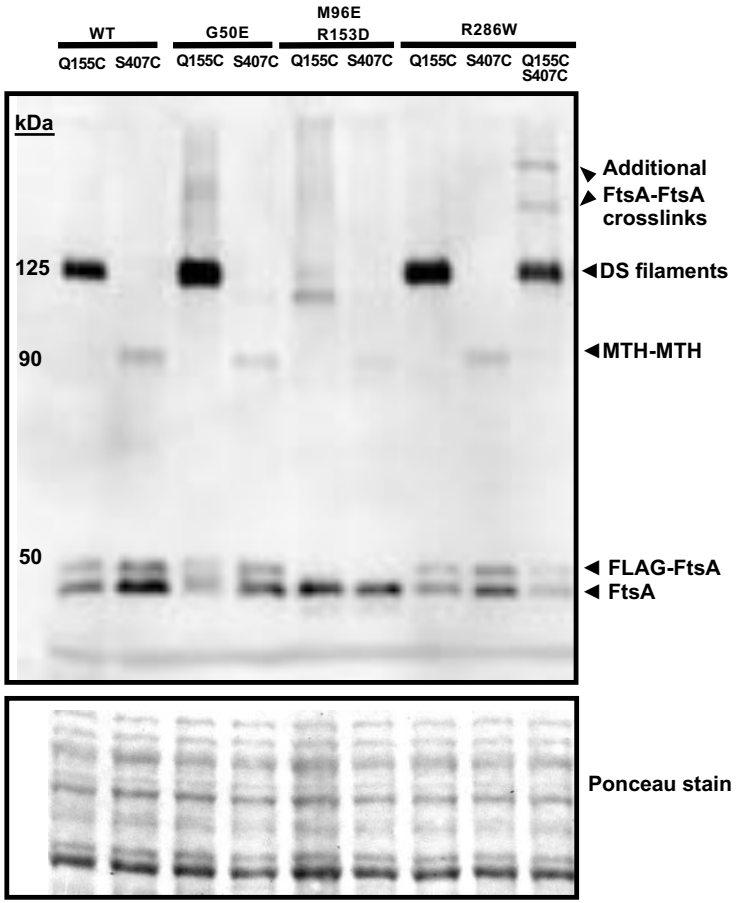
WT
G50E
M96E
R153D
R286W
Q155C S407C
Q155C S407C
Q155C S407C
Q155C S407C
Q155C
S407C
kDa
125
90
50
Additional
FtsA-FtsA
crosslinks
DS filaments
MTH-MTH
FLAG-FtsA
FtsA
Ponceau stain

Fig. 4

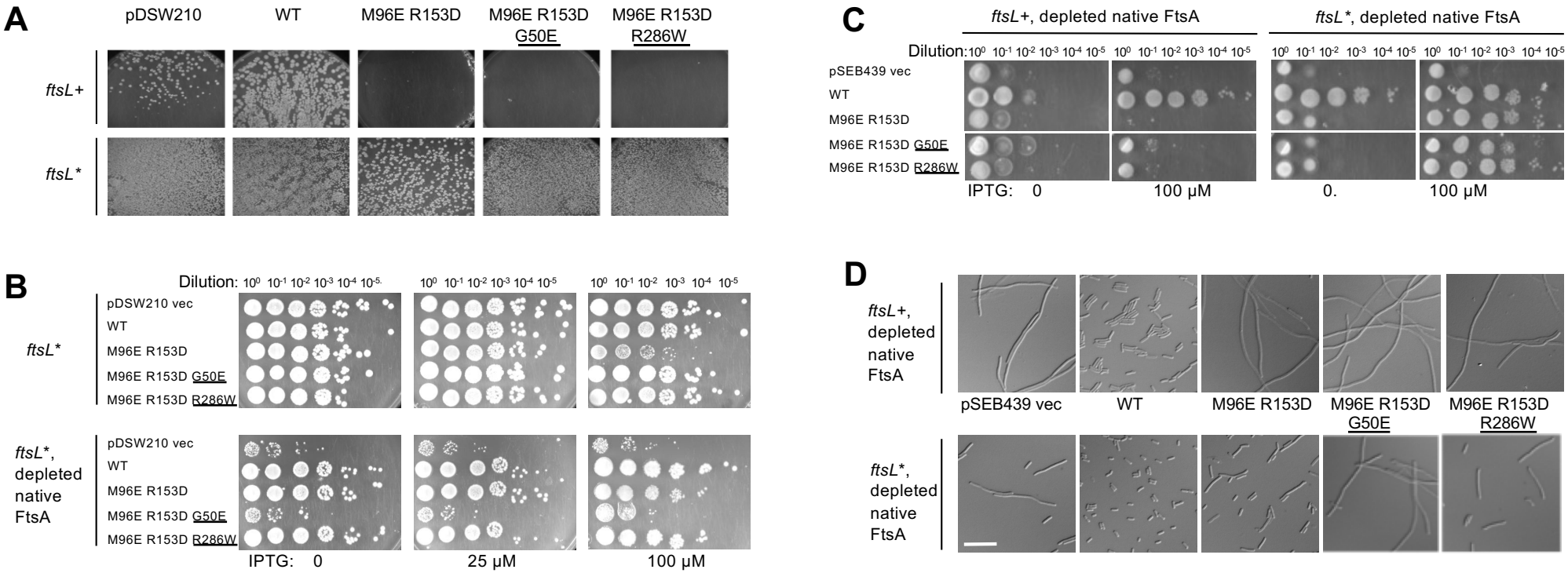
A
pDSW210
WT
M96E R153D
M96E R153D G50E
M96E R153D R286W
ftsL+
ftsL*
B
Dilution: 10^0 10^-1 10^-2 10^-3 10^-4 10^-5
pDSW210 vec
WT
M96E R153D
M96E R153D G50E
M96E R153D R286W
ftsL*
ftsL*, depleted native FtsA
IPTG: 0
25 μM
100 μM
C
ftsL+, depleted native FtsA
ftsL*, depleted native FtsA
Dilution: 10^0 10^-1 10^-2 10^-3 10^-4 10^-5
pSEB439 vec
WT
M96E R153D
M96E R153D G50E
M96E R153D R286W
IPTG: 0
100 μM
0.
100 μM
D
ftsL+, depleted native FtsA
pSEB439 vec
WT
M96E R153D
M96E R153D G50E
M96E R153D R286W
ftsL*, depleted native FtsA

Fig. 5

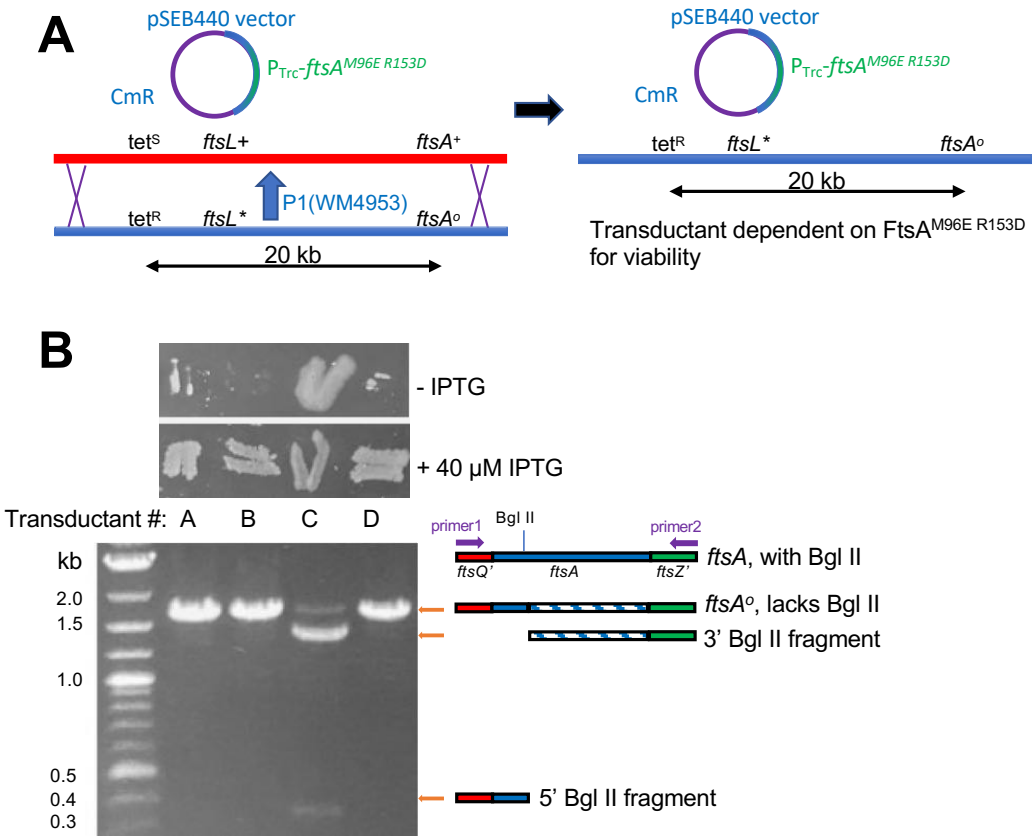
A
pSEB440 vector
CmR
PTrc-ftsAM96E R153D
tetS
ftsL+
ftsA+
P1(WM4953)
tetR
ftsL*
ftsAo
20 kb
pSEB440 vector
CmR
PTrc-ftsAM96E R153D
tetR
ftsL*
ftsAo
20 kb
Transductant dependent on FtsAM96E R153D
for viability
B
- IPTG
+ 40 μM IPTG
Transductant #: A B C D
kb
2.0
1.5
1.0
0.5
0.4
0.3
primer1
Bgl II
primer2
ftsQ'
ftsA
ftsZ'
ftsA, with Bgl II
ftsAo, lacks Bgl II
3' Bgl II fragment
5' Bgl II fragment

Fig. 6

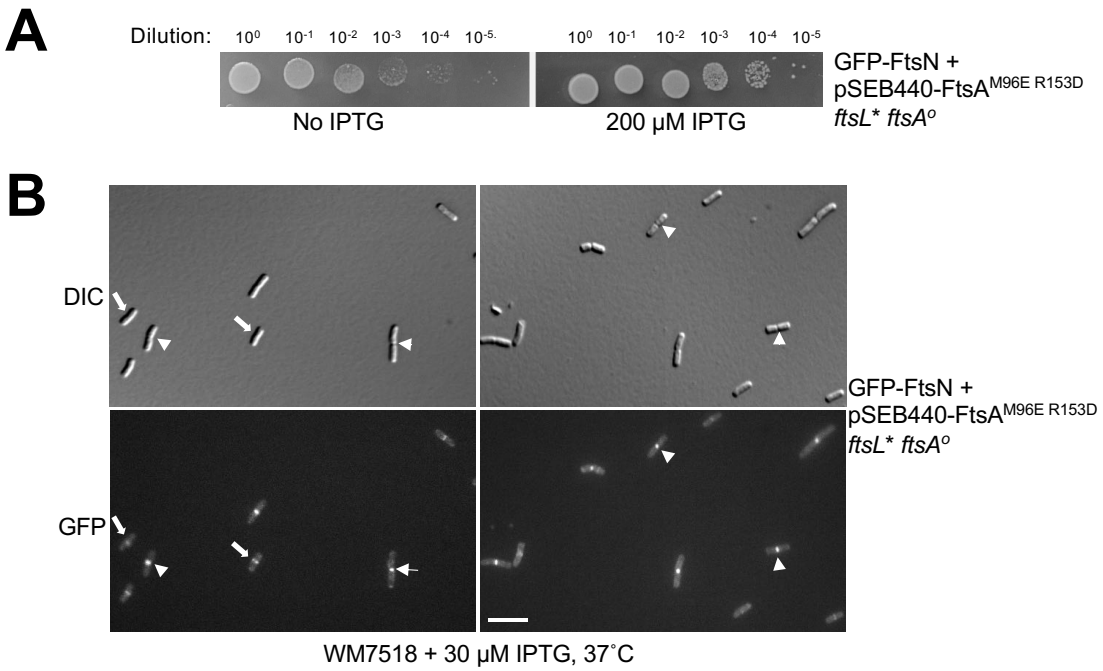
A
Dilution:
10^0 10^-1 10^-2 10^-3 10^-4 10^-5
10^0 10^-1 10^-2 10^-3 10^-4 10^-5
No IPTG
200 μM IPTG
GFP-FtsN +
pSEB440-FtsA^M96E R153D
ftsL* ftsA^o
B
DIC
GFP
GFP-FtsN +
pSEB440-FtsA^M96E R153D
ftsL* ftsA^o
WM7518 + 30 μM IPTG, 37˚C

Fig. 7

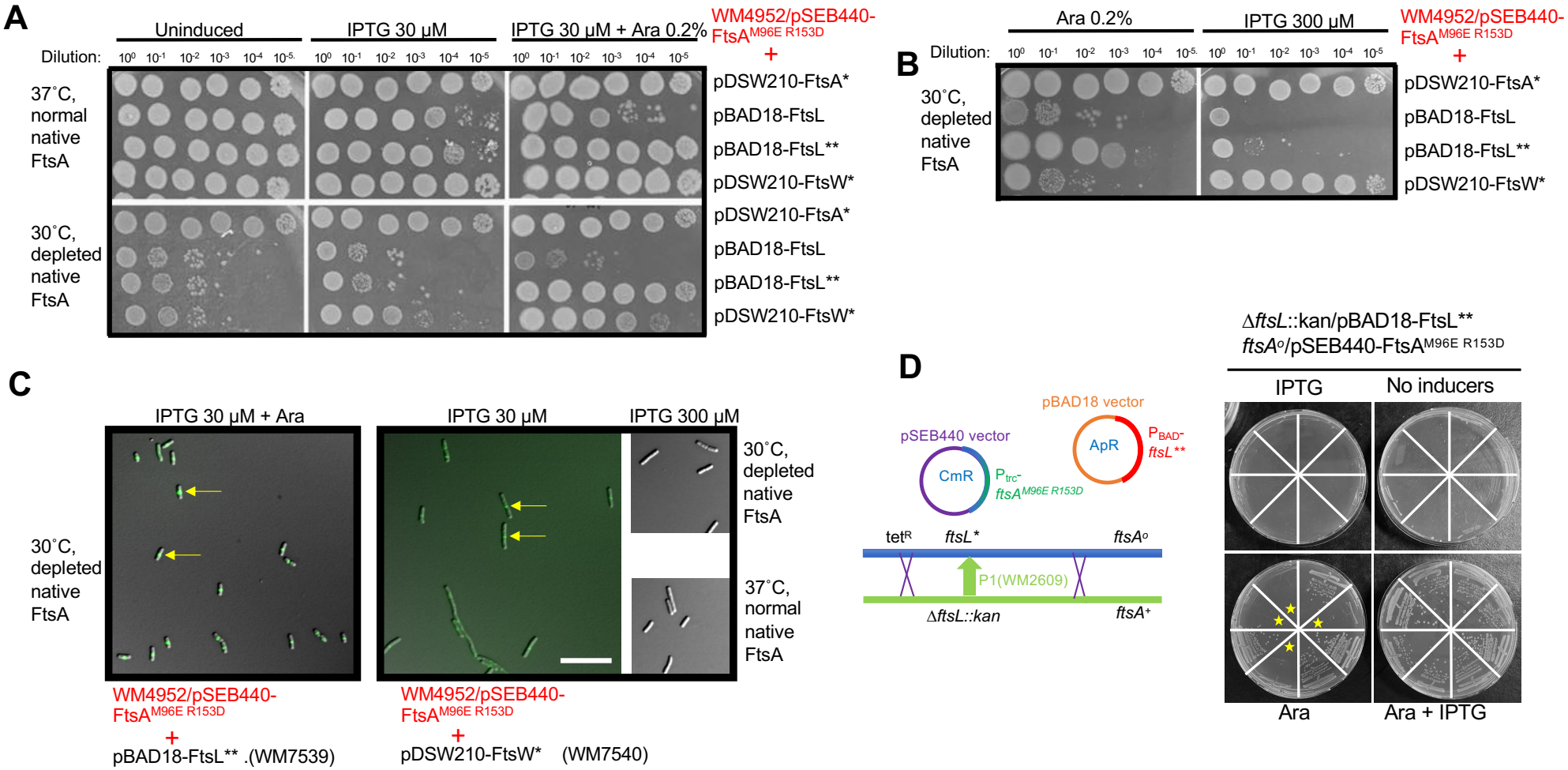
A
Uninduced
IPTG 30 μM
IPTG 30 μM + Ara 0.2%
Dilution:
10⁰ 10⁻¹ 10⁻² 10⁻³ 10⁻⁴ 10⁻⁵
37˚C, normal native FtsA
30˚C, depleted native FtsA
WM4952/pSEB440-FtsA M96E R153D
+
pDSW210-FtsA*
pBAD18-FtsL
pBAD18-FtsL**
pDSW210-FtsW*
pDSW210-FtsA*
pBAD18-FtsL
pBAD18-FtsL**
pDSW210-FtsW*
B
Ara 0.2%
IPTG 300 μM
Dilution:
10⁰ 10⁻¹ 10⁻² 10⁻³ 10⁻⁴ 10⁻⁵
30˚C, depleted native FtsA
WM4952/pSEB440-FtsA M96E R153D
+
pDSW210-FtsA*
pBAD18-FtsL
pBAD18-FtsL**
pDSW210-FtsW*
C
IPTG 30 μM + Ara
IPTG 30 μM
IPTG 300 μM
30˚C, depleted native FtsA
30˚C, depleted native FtsA
37˚C, normal native FtsA
WM4952/pSEB440-FtsA M96E R153D
+
pBAD18-FtsL** .(WM7539)
WM4952/pSEB440-FtsA M96E R153D
+
pDSW210-FtsW* (WM7540)
D
pBAD18 vector
pSEB440 vector
ApR
P BAD- ftsL**
CmR
P trc- ftsA M96E R153D
tetR
ftsL*
ftsAo
P1(WM2609)
ΔftsL::kan
ftsA+
ΔftsL::kan/pBAD18-FtsL**
ftsAo/pSEB440-FtsA M96E R153D
IPTG
No inducers
Ara
Ara + IPTG

Fig. 8

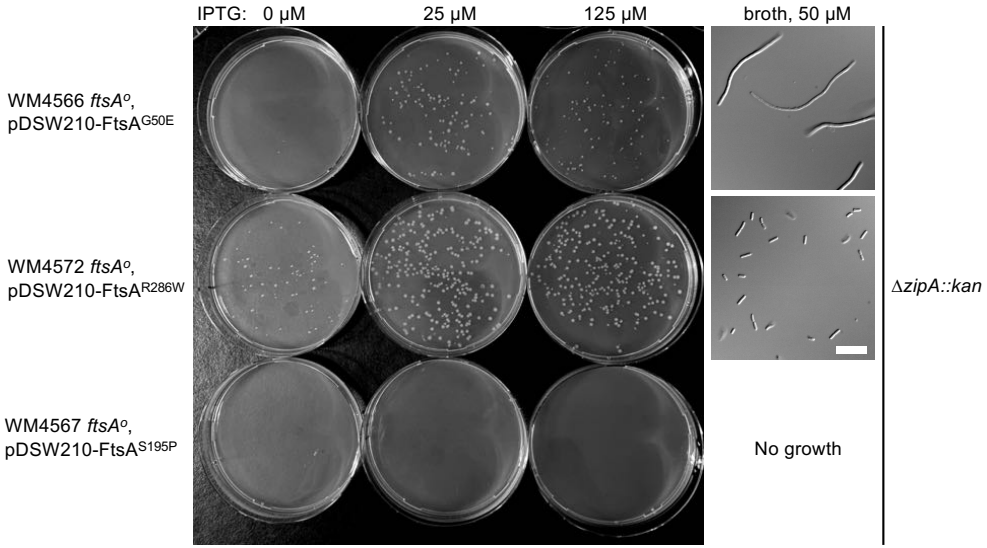
IPTG: 0 μM
25 μM
125 μM
broth, 50 μM
WM4566 *ftsA*^{o}, pDSW210-FtsA^{G50E}
WM4572 *ftsA*^{o}, pDSW210-FtsA^{R286W}
WM4567 *ftsA*^{o}, pDSW210-FtsA^{S195P}
No growth
Δ*zipA::kan*

Fig. 9

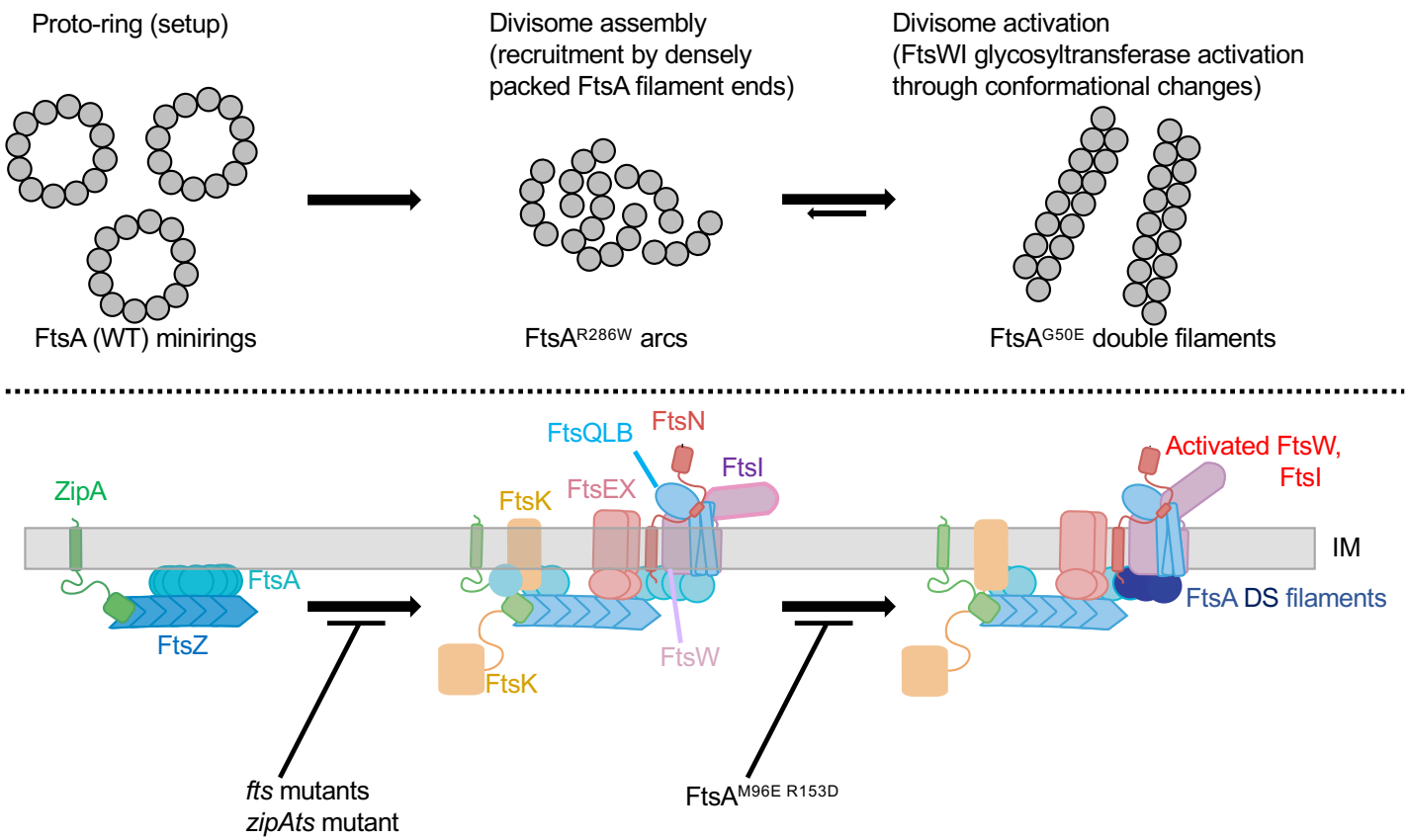
Proto-ring (setup)
Divisome assembly
(recruitment by densely
packed FtsA filament ends)
Divisome activation
(FtsWI glycosyltransferase activation
through conformational changes)
FtsA (WT) minirings
FtsA^{R286W} arcs
FtsA^{G50E} double filaments
ZipA
FtsA
FtsZ
FtsK
FtsQLB
FtsN
FtsEX
FtsI
FtsK
FtsW
Activated FtsW,
FtsI
IM
FtsA DS filaments
fts mutants
zipAts mutant
FtsA$^{M96E\ R153D}$

Fig. 10